UQAC
Université du Québec
à Chicoutimi

Enhancing Winter Runway Safety:
Development of a tool for Friction Measurement in laboratory

By

María Lucia Loaiza Osorio

Under supervision of Prof. Gelareh Momen and co-supervision of Prof. Jean-Denis Brassard and Prof. Jean Perron

Dissertation presented to the Université du Québec à Chicoutimi with a view to obtaining the master's degree in engineering (3708)

Board of examiners:
Professor Dilip Sarkar, department of Applied Sciences at UQAC, President of the board of examiners
Professor Éric Villeneuve, Department of Applied Sciences at UQAC, Internal Member of the Board
Professor Gelareh Momen, Department of Applied Sciences at UQAC, Internal Member of the Board
Professor Jean-Denis Brassard, Department of Applied Sciences at UQAC, Internal Member of the Board
Professor Mario Marchetti, Department of Applied Sciences at UQAC, Internal Member of the Board

Québec, Canada.

Résumé

En hiver, les opérations aériennes deviennent difficiles en raison des désagréments causés par les conditions météorologiques. Les sorties de piste d'aéronefs sont en tête de liste des incidents liés aux opérations au sol. Les performances de freinage des avions diminuent en raison des contaminants hivernaux, ce qui peut entraîner la sortie de l'avion de la piste désignée lors du décollage ou de l'atterrissage, représentant ainsi un risque de sécurité important dans l'aviation. Bien que ces incidents se produisent tout au long de l'année, leur fréquence augmente en hiver. Les statistiques montrent que les sorties de piste en 2019 ont entraîné des pertes financières mondiales de 4 milliards de dollars. Toutefois, la diversité des dispositifs et des méthodologies utilisées dans l'industrie aéronautique engendre une variabilité des résultats, rendant leur comparaison complexe et parfois incohérente.

Dans ce contexte, il est essentiel de développer des outils de mesure fiables et standardisés pour mieux évaluer l'adhérence des pistes en conditions hivernales. Cette thèse présente le dispositif Multi-Tool Apparatus (MTA), utilisée pour la mesure de l'adhérence de la glace. Sa nouvelle fonctionnalité de mesure de la friction est élaborée pour simuler l'interaction entre les roues d'avion et les pistes contaminées. Le MTA a mesuré la friction dans des scénarios de surface secs et glacés à l'aide d'une fixation en caoutchouc et d'échantillons de béton représentatives des conditions des pistes canadiennes. Les résultats respectent les réglementations et les valeurs de friction détaillées par l'Indice Canadien de Friction des Pistes ainsi que les modèles théoriques, validant ainsi l'efficacité et les performances de l'appareil.

Les résultats de multiples tests de friction effectués à différentes charges et vitesses ont permis de déterminer les réglages opérationnels idéaux pour le MTA afin d'obtenir des mesures de friction cohérentes et précises. Les résultats ont montré qu'une charge de 226 N et une vitesse de 0,025 km/h sont optimales pour faire fonctionner le MTA lors des tests de friction. De plus, en addition aux tests sur des surfaces sèches et glacées, nous avons introduit un produit de dégivrage de piste afin de tester la capacité de cet appareil à évaluer l'impact de ces fluides couramment utilisés pour la maintenance hivernale.

Autre objectif clé de cette étude a été de développer un modèle mathématique pour décrire le coefficient de frottement entre des surfaces glissantes en utilisant les résultats du MTA. Ce modèle a amélioré notre compréhension des dynamiques expérimentales et confirme la fiabilité du MTA en tant que testeur de frottement, conformément aux théories établies. Basé sur la première loi d'Amontons et le modèle d'adhésion et de labourage de Dowson, ce modèle fournit des prédictions avec des marges d'erreur inférieures à 8 % pour la glace, le béton sec et humide, atteignant une précision supérieure à celle du modèle linéaire.

Le dispositif MTA comble les lacunes identifiées lors de la revue de la littérature, où l'appareil de laboratoire le plus utilisé, qui correspond le mieux aux réglementations, fournit des données sous forme de British Pendulum Number (BPN), lesquels peuvent être difficiles à corréler avec les coefficients de friction. Le MTA offre une approche plus pratique, en mesurant directement le coefficient de friction dans diverses conditions environnementales et de surface.

Cet appareil modulaire peut mesurer toute surface plane, interchanger des accessoires pour simuler plusieurs scénarios et propose une procédure de test simple. Il offre une voie prometteuse pour les laboratoires de tests de friction, les RDPs et d'autres scénarios importants impliquant la sécurité aérienne en hiver.

Mots clés: Friction, Résistance au glissement, Excursion de piste, Produits de dé-icing de piste, Béton, Sécurité aérienne, Conditions hivernales, Tribologie, Performance de freinage, Bruine glaciale.

Abstract

During winter, aircraft operations become challenging due to the inconveniences that extreme cold weather conditions cause. Runway excursions are first on the list when we talk about incidents in ground operations. Aircraft braking performance decreases due to winter contaminants making the aircraft exit the designated runway surface during takeoff or landing, which poses a significant safety risk in aviation. Although these incidents persist throughout the year, their frequency increases during winter. The statistics indicate that 2019 runway excursions contributed to global financial losses of $4 billion. Yet, the aviation industry faces challenges due to the various devices and methodologies, resulting in inconsistent and often incomparable results.

Addressing these inconsistencies requires reliable and standardized measurement tools to better assess runway conditions and mitigate safety risks. This dissertation introduces the Multi-Tool Apparatus (MTA), initially used to measure ice adhesion This device, with its new frictional modality, is designed to simulate the interaction between aircraft wheels and icy runways. The MTA measured friction under dry and icy scenarios using a rubber attachment and concrete samples that replicated Canadian runway conditions. The results meet the regulations and friction values detailed by the Canadian Runway Friction Index (CRFI) and theoretical models, validating the device's effectiveness and performance.

The response from multiple friction tests at different normal forces and velocities determined the ideal operational settings for the MTA to obtain consistent and precise friction measurements. The results indicated that a normal force of 226 N and velocity of 0,025 km/h are optimal for operating the MTA during the friction tests. Also, in addition to testing on different winter conditions, we introduced Runway De-icing Product (RDP) in its de-icing and anti-icing mode to test the ability of this device to perform friction tests with fluids commonly used for winter maintenance.

As a key objective of this study, we developed a mathematical model to simulate the friction coefficient between sliding surfaces using the MTA's results. This model improved our understanding of the experimental dynamics and confirms the reliability of the MTA as a friction tester in accordance with established theories. The model, built on Amontons' first law and Dowson's adhesive and ploughing framework, provides predictions with error margins of less than 8% for ice, dry and wet concrete, achieving higher accuracy than the linear model.

The MTA device fills the gaps found in the literature review, where the most used laboratory device that fits better the regulations delivers data in the form of British Pendulum Number (BPN), which can be difficult to correlate with friction coefficients, the MTA offers a more practical approach, enabling the direct measurement of the coefficient of friction under various environmental and surface conditions.

This device can measure any flat surface, interchange attachments to simulate more than one scenario, and has a simple testing procedure and a promising path in the testing laboratory of friction, RDPs and other significant scenarios that imply aviation safety during winter.

Key words: Friction, Skid resistance, Runway excursion, Runway de-icing products, Concrete, Aviation safety, Winter conditions, Tribology, Braking performance, Freezing drizzle.

Table of Content

List of figures

List of tables

List of Equations

List of Abbreviations

AMIL	=	Anti-icing Materials International Laboratory
APD	=	Aachen Polishing Device
ASTM	=	American Society of Testing Materials
BPT	=	British Pendulum Tester
BPN	=	British Pendulum Number
CRFI	=	Canadian Runway Friction Index
CFME	=	Continuous Friction Measuring Equipment
DOT	=	Department of Transportation
DEC	=	Decelerometers
DFT	=	Dynamic Friction Tester
DC	=	Direct Current
EN	=	European Standard
ERD	=	Electronic Recording Decelerometer
FAA	=	Federal Aviation Administration
FHWA	=	Federal Highway Administration
FN	=	Friction Number
GRF	=	Global Reporting Format
ISO	=	International Organization for Standardization
ICAO	=	International Civil Aviation Organization
IMAG	=	Automatic Slip Measurement Instrument
JWRFMP	=	Joint Winter Runway Friction Measurement
LFC	=	Longitudinal Friction Coefficient
MPD	=	Mean Profile Depth
MTA	=	Multi-Tool Apparatus
MVD	=	Mean Volumetric Diameter

NASA	=	National Aeronautics and Space Administration
PWS	=	Polishing Wehner/Schulze
PFM	=	Pavement Friction Management
PICP	=	Permeable Interlocking Concrete Pavement
RASG-PA	=	Regional Aviation Safety Group — Pan America
RDP	=	Runway De-icing Products
RWY	=	Runway
RwyCC	=	Runway Condition Code
SCRIM	=	Sideways Force Coefficient Routine Investigation Machine
SFC	=	Side-Force Coefficient
TC	=	Transport Canada
UQAC	=	University of Quebec at Chicoutimi
UK	=	United Kingdom
USA	=	United States

List of Symbols

A_0	=	Sum of the area of indenting asperities perpendicular to the direction of sliding
A_{real}	=	Real contact area
$F_{\parallel}$	=	Tangential force (Friction force)
$F_{\perp}$	=	Normal force
F_{ploug}	=	Ploughing force
F_{sh}	=	Shearing force
H'	=	Yield stress of rubber
H	=	Yield stress of the hardest material
L	=	Contact area length
W	=	Contact area width
α	=	Angle of flattering
β	=	Yield stress ratio between the slider's materials
μ	=	Friction coefficient
μ^*	=	Constant of modelling
θ_1	=	Angle to the direction of the sliding for conical asperities
a	=	Constant of modelling
b	=	Radius of the deformed portion of the conical asperity
h	=	height of the deformed portion of the conical asperity
l	=	Conical asperity height
r	=	Conical asperity radius
s	=	Tangential stress needed to shear the junction

Dedication

To God, who gave me the ability to believe in my dreams and the confidence to know that we would fight for them together.

To my husband, for his unconditional support and for making me feel capable of anything.

To my parents, who have always given me their best and for their total dedication to our family, thank you for raising me as a strong woman.

To my sisters, for inspiring me with their journeys.

To my supervisors, for giving me this opportunity and for believing in me.

Acknowledgment

I would like to express my sincere gratitude to my supervisor, Professor Gelareh Momen, for her support throughout this process and her invaluable mentorship. Thank you for giving me the opportunity to be part of the laboratory and for inspiring me with your remarkable journey as a leading woman in engineering.

I extend my heartfelt thanks and admiration to Professor Jean-Denis Brassard for introducing me to the field of research when he accepted me as his Mitacs intern, for his constant guidance and patience at every step, and for the valuable lessons he has imparted, both professionally and personally.

I also want to thank Professor Jean Perron for sharing his passion for science and engineering with me. His continuous mentorship and willingness to help have been invaluable. I am in awe of your brilliance.

I would like to acknowledge my lab colleagues Claire Charpentier, Sanae Benaissa, and Samaneh Keshavarzi for all the happy moments and support, as well as for sharing their advice and experiences with me.

I sincerely appreciate the collaboration and support of the professionals and technicians at the Anti-Icing Materials International Laboratory, especially to Professor Derek Harvey, Ms. Caroline Blackburn, Ms. Shan Yang, Mr. Carol Mercier, Mr. Patrice Rondeau and Mr. Jean-Philippe Gagné.

I would also like to express my sincere appreciation to Aéroports de Montréal, the Natural Sciences and Engineering Research Council of Canada (NSERC), the Consortium for Research and Innovation in Aerospace in Québec (CRIAQ), MITACS, and the Ministère de l'Économie et de l'Innovation du Québec for providing the financial support that made my research possible.

Last but not least, I would like to thank my friends who became my family during my studies, Isaac Laguna, Andrés Cardona, Denisse Alano, Carlos Cuao, Abraham Serena, Elizabeth Peña, and João Pedro.

Chapter 1: Introduction

1.1 Problem Definition

Data from 2013 to 2022 reveals that 23% of commercial aviation accidents stem from runway excursions [1]. These are among the high-risk categories outlined in the International Civil Aviation Organization (ICAO) Global Aviation Safety Plan (GASP, Doc 10004). The Regional Aviation Safety Group — Pan America (RASG-PA), in their Annual Safety Report 2023, referred to runway excursions as the third leading cause of aviation accidents (Figure 1) [2]. In 2024, tail strikes were the most common type of accident in North America, followed by runway damage and runway excursions [3].

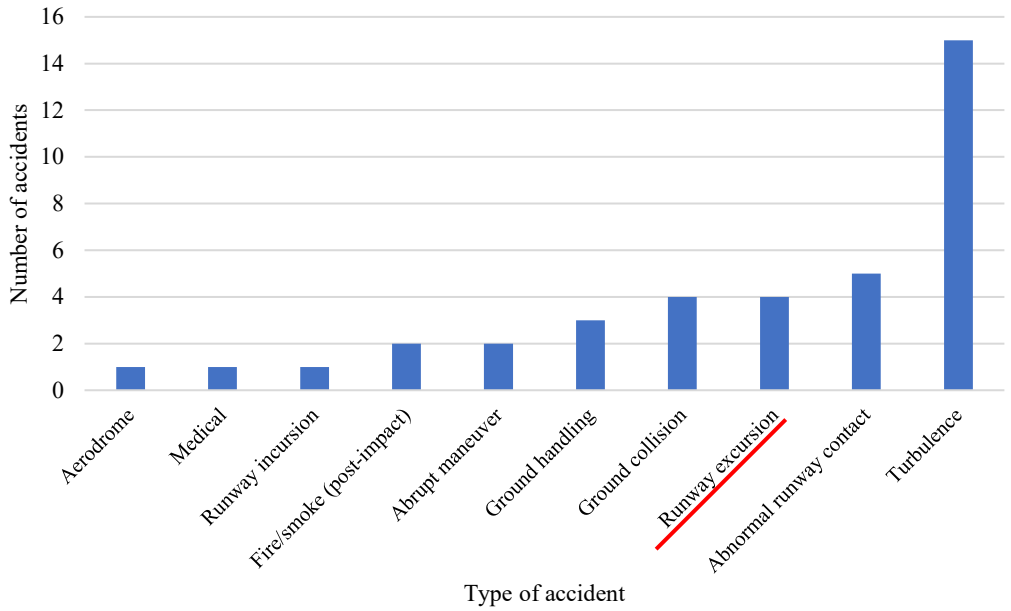

Figure 1: Accidents by category in 2023. Inspired on [1].

The leading types of accidents among airliners operating worldwide, in both passenger and cargo services, in 2022, were turbulence, runway excursions, and ground damage, according to the 2022 Safety Report by the Flight Safety Foundation [4]. This report reviews accidents on global airliners and corporate jets from 2017 to 2022 and shows that more than 50% of airliners accidents were attributed to five high-risk accident types, including runway excursions [4].

Runway excursion refers to any occurrence or situation, whether realized or potential, in which an aircraft departs from the designated confines of the runway or the operational area of an aerodrome or specified landing area without achieving lift-off [5]. In the year 2019, the aviation sector experienced a financial impact of 4 billion dollars attributed to such occurrences, primarily concentrated in the winter season when runway surfaces were contaminated by elements such as snow, slush, ice, brine, or water [6]. Inadequate braking performance stands as primary contributing factor amplifying runway excursions, especially under winter conditions. To ensure appropriate and precise braking action, pilots require accurate and detailed information about runway surface conditions. This concern arises due to the intricate nature of accurately gauging runway friction, a challenge that persists despite concerted efforts to measure it with the utmost precision [7, 8].

In 2021, Canada adopted the Global Reporting Format (GRF) to enhance flight safety and comply with the International Civil Aviation Organization's (ICAO) call for regulated and enhanced reporting methods for runway surface conditions, leading to this initiative [5]. The GRF principle means that the airport staff checks the runway's surface condition whenever there is water, snow, slush, ice, or frost on an active runway. Based on their assessment, they assign a Runway Condition Code (RWYCC) and provide a description of the surface. This information helps the flight crew to figure out how the runway's condition might affect the plane's performance during takeoff and landing [13].

Currently, there are no laboratory methods that fully align with regulatory standards, with the British Pendulum Test (BPT) being the most commonly used for correlating with the GRF [6]. However, the BPT provides a specific measurement, the British Pendulum Number (BPN), which complicates a direct comparison with the friction coefficients required by standards or results from other testing equipment. Furthermore, the BPT is less effective when contaminants, such as snow, are present, which limits its applicability for certain laboratory tests.

Measuring friction in a controlled laboratory environment is crucial for evaluating runway conditions and improving winter maintenance strategies. It helps assess the effectiveness of de-icing products and determine the appropriate amount needed based on specific surface conditions. Laboratory

testing also enables better correlation with real-world runway scenarios, contributing to more accurate predictions and enhanced safety in aviation operations.

1.2 Objectives

The primary objective of this research is to develop and to propose a laboratory methodology for measuring friction that simulates the interaction between aircraft wheels and a runway contaminated by icing and or snowing precipitations. This approach is based on insights from Montreal airports and relevant literature. Building upon the experimental results obtained from the developed laboratory friction device and the insights from the literature review, this research will also focus on validating the proposed device through a comprehensive mathematical model. The specific sub-objectives of this research are outlined below:

- Identify key gaps and needs in the aviation industry concerning field and laboratory friction measurement devices.
- Adapt the MTA to measure friction under simulated winter conditions, ensuring compliance with current Canadian and international standards and regulations.
- Assess the performance of the friction device in the presence of RDP's.
- Develop a mathematical model to validate the friction device's performance, demonstrating its consistency with friction theory.

1.3 Methodology

This research focuses on developing and implementing a friction measurement apparatus at the University of Quebec at Chicoutimi within the Anti-icing Materials International Laboratory (AMIL). The core instrument for this study is the Multi-Tool Apparatus, initially designed for ice adhesion measurement and adapted to replicate the tribological system created by the aircraft wheels and the runway surface during winter conditions.

The second chapter asses different friction measurement devices, methodologies, regulations, and standards. This literature review allowed us to assess the feasibility of incorporating these standards into the

laboratory setup, optimizing the MTA for accurate simulation of real-world runway conditions, and filling the gaps between theoretical concepts and practical application in winter aviation operations.

To simulate the target frictional scenario, the ice scraper normally used with the MTA was replaced with a rubber attachment, ensuring optimal contact with the tested substrate. The MTA characterization was then performed, including load cell calibration and a speed check test. Since the device operates at different frequencies, this test was necessary to determine the corresponding speed values for each frequency setting.

Several normal force and velocity tests were conducted to identify the most suitable settings for the MTA with the concrete specimens, ensuring optimal conditions for obtaining accurate and representative results. Runway anti-icing fluids were then introduced to evaluate the MTA's performance under conditions closely replicating real-world scenarios. Additionally, the rubber piece's surface roughness was measured using a 3D optical profilometer, which provided surface geometry, texture analyses, and flattening angles.

Finally, the MTA's accuracy in measuring friction under various conditions was validated using a mathematical model. This model introduces important frictional descriptions, such as Amontons' laws and Dowson principal models, and used the experimental data obtained from the friction test, focusing on a roughness conic model, the lubrication and friction on solids, and the effect of yield strength of materials in contact. Figure 2 summarizes the methodology of this research.

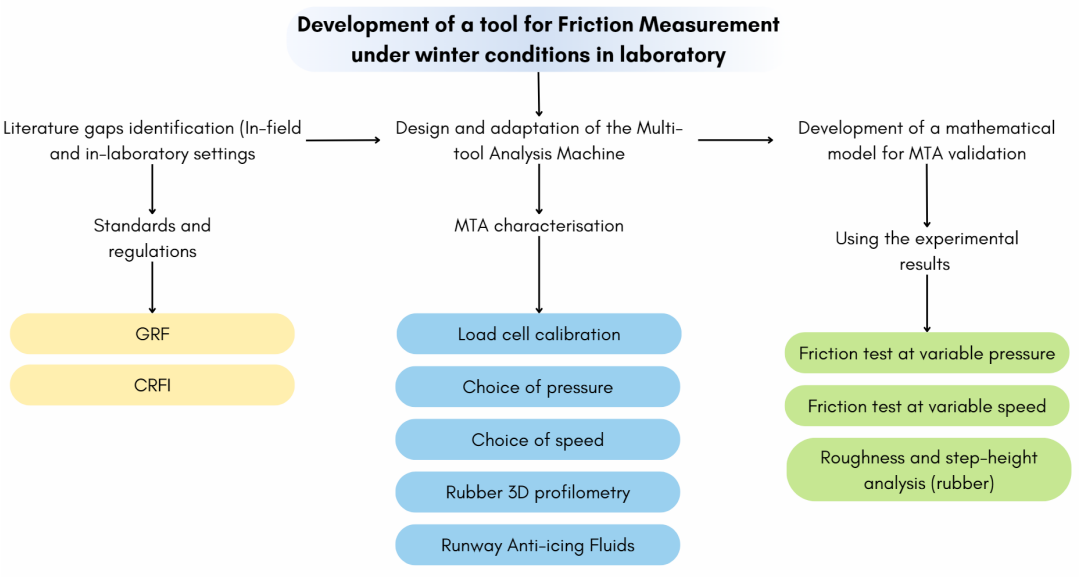

Figure 2 : Summary of the Research Methodology: Yellow – Literature Review, Blue – Methodology, Green – Results and Discussion

1.4 Originality Statement

The originality of this research project lies in two key aspects:

- The focus on airport runway friction under winter conditions within a laboratory setting.
- The development of a methodology utilizing a laboratory tool designed for accurate friction measurement in these conditions

First, the frictional interaction between aircraft wheels and runways is a critical tribological system that directly impacts aviation safety. There is an urgent need for comprehensive laboratory tools that measure the friction coefficient under a controlled environment, especially simulating winter conditions with the conjunction of runway de-icing products. Despite airport operations being a driving force for the economy, friction measurements in such scenarios have yet to be thoroughly explored. The research gap is evident, as the existing British Pendulum Tester (BPT), the most commonly used device for correlating with the GRF in winter conditions, operates under pure sliding conditions. As a result, it yields results in the British Pendulum Number (BPN), which may not fully capture the complex frictional interactions occurring during aircraft braking. When comparing or correlating the BPN with other methodologies or real-world field data, there is no direct way to do so, as most devices and standards provide data in terms of the friction coefficient. As a result, the process becomes less practical, less efficient, and non-representative.

On the other hand, various studies have made significant attempts to measure runway friction coefficients, but the majority remain in exploratory phases without involving any practical experimentation. Also, when they achieve the design stages, most are usually not fully aligned with current Canadian airport standards.

This research introduces the Multi-Tool Apparatus' adaptation as an innovative friction measurement apparatus to fill those gaps. The MTA stands out for its ability to simulate the interaction between aircraft wheels and contaminated runway surfaces by applying various regular forces and velocities and utilizing different slider attachments to replicate operational conditions.

1.5 Memoire Outline

This research project is divided in five chapters, each carefully sectioned to provide clear information to the reader and to maintain a consistent flow of information. This subsection provides a summary of the upcoming chapters.

Chapter 2

This chapter presents the theoretical foundation of this study, guiding the reader from the broad concept of tribology to more specific terms, such as skid resistance measurement methodologies. It covers all the crucial and relevant ideas to provide a strong foundation for the theories and recent advancements central to this research.

With this robust foundation, the reader is introduced to different methodologies for measuring skid resistance under winter conditions, specifically within the aviation field. These methodologies are divided into laboratory and in-field testing methods, which are then compared.

At the end of this chapter, there is a section focused on interpreting friction data from different devices using real studies and data, aiming to compare them and to illustrate how airport operators today select the appropriate device to meet their specific needs.

Chapter 3

The third chapter describes the methodology and materials used in this study. It includes MTA's components, the testing environment, and the various tests conducted to characterize and to evaluate the MTA's performance. Additionally, it provides a detailed explanation of the velocity and normal force ranges utilized during testing to describe the device's capabilities.

In Chapter 3, the rubber attachment, which simulates aircraft wheels, is thoroughly analyzed using 3D profilometry to investigate its surface roughness and texture. The concrete specimens selected to replicate the airport runway are also described in detail, along with the simulated winter precipitations. Furthermore, this chapter presents the runway de-icing products tested during the experiments and describes the methodology employed, ensuring a clear understanding of the procedures and conditions.

Chapter 4

This chapter presents a comprehensive overview of the results obtained from the tests previously introduced, with an in-depth discussion and analysis of collected data. It begins with the presentation of the load cell calibration, followed by detailed friction tests conducted using the MTA. These tests were divided into two groups: one set was performed with variable normal force and the other with variable velocity. This approach allowed us to identify the optimal velocity and normal force settings that enhance the MTA's performance.

This chapter then displays the results of the roughness measurements conducted using 3D profilometry, with multiple line profiles captured along the rubber surface to thoroughly analyze its texture. The outcomes of the tests involving anti-icing fluids are also presented, along with a detailed interpretation of these findings. At the end of this chapter is the mathematical model step-by-step procedure developed, integrating the theoretical framework of friction and our experimental data, ensuring that the findings align with established friction theory.

Chapter 5

In the final chapter of this thesis, the reader will be provided with a comprehensive overview of all preceding chapters, highlighting the most relevant insights and key findings from each section. This chapter summarize the problematic, context and methodologies taken throughout this research journey. Also, future research recommendations, and suggestions for further exploration in friction measurement methodologies and the application of the MTA are presented.

Chapter 2: Literature Review on Skid Measurement

2.1 Introduction

Runway friction measurement mainly aims to ensure take-off and landing safety [9]. Friction measurements frequently entail three elements: the measuring tire, the runway surface, and a contaminant that interacts with both the tire and the surface, such as frozen precipitations [10]. A runway is contaminated if its operational surface incorporates other substances, such as water, slush, loose snow, wet snow, slush ice, frost, or other deposits, such as sand, mud, or dust, that cover more than 25% of its surface [6]. When the surface is contaminated, the skid resistance, or pavement friction level, decreases, which is a significant challenge for pilots, potentially leading to a higher rate of runway excursions, as mentioned in the previous chapter [11].

When discussing the skid resistance of a runway surface, our primary focus is how much the surface helps the tires grip the road and thus creates friction. The skid resistance measures the interaction effectiveness between the pavement surface and the aircraft tires [12]. Due to its pivotal role in ensuring safe runways, skid resistance becomes a crucial element that requires careful consideration when making decisions about its maintenance. Numerous methods, mainly derived from the American Society of Testing Materials (ASTM) test methods, have been developed to assess runway surface braking efficiency and condition [13].

This chapter comprehensively analyzes diverse in-situ and laboratory skid resistance measuring devices of runway concrete under winter conditions. We classify the apparatus based on their principle with the associated standard, measurement index, their advantages, limitations, and specific applications. Then, we discussed some articles' insights and methodologies where they used these devices to measure skid resistance under winter conditions. Finally, based on different studies, we identified that the best way to correlate the current skid resistance values is by their interfacial condition (dry, wet, ice), where the highest value of each range represents the dry condition, and zero is the most dangerous.

2.2 Tribology

In 1966, Jost HP [14] introduced the word “tribology” by amalgamating the Greek root “tribe,” which means “rubbing,” with the suffix “-logy,” denoting “the study of.” This term covers the exploration of friction, wear, lubrication, and adhesion while also considering the interplay between scientific principles and economic dynamics of the relatively moving contact surfaces [15, 16]. The genesis of tribology has its roots in the difficulties faced in operating drive systems. This discipline delves into how surfaces interact, which is influenced by the physical and mechanical characteristics of those surfaces and the conditions under which they operate. Given its multifaceted nature as a complex field, tribology is closely tied to numerous real-world applications and practical uses, making it challenging to develop comprehensive theoretical models for every situation. As a result, there are limited opportunities to create theoretical formulations that apply to the full range of tribological scenarios [17].

When assessing the interaction between two or more surfaces in contact, the concept of a tribological system arises, with three essential parts involved: friction pairs (surface parameters, chemical reactivity, mechanical properties, etc.), lubricant or contact (rheological properties), and the surrounding medium or working environment (temperature, humidity, exposure duration, operational time, aging effects, etc.) as is shown in Figure 3. Tribological systems are influenced by various factors, such as relative speed, movement direction, and average load. This has resulted in the utilization of diverse data sources and the development of numerous theoretical frameworks in the field of tribological research [18-20].

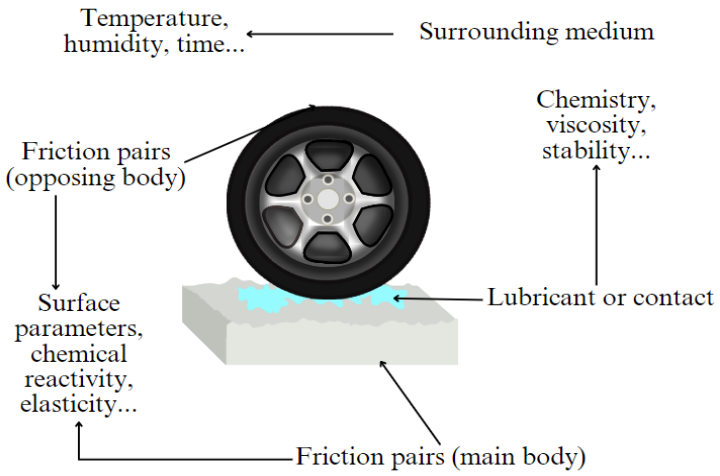

Figure 3 : Tribological System Representation: Key Factors Affecting Tire-Surface Interaction

The subsequent sections comprehensively present and elucidate the fundamental concepts and principles of pavement friction. In these sections, we detail the factors that influence friction and meticulously expound upon the domain of skid resistance.

Pavement Friction in Roadway Applications

The following section primarily addresses pavement friction in the context of road surfaces, emphasizing the challenges associated with skid resistance and surface maintenance. The friction analysis plays a crucial role in regulating road surfaces' economic and property aspects. Monitoring the friction coefficient and focusing on ice prevention can lead to significant cost savings. In Class A airfields, where all operations follow instrument flight rules and aircraft are strictly managed under air traffic control clearance and separation, the worldwide annual use of anti-icing chemicals was reduced by approximately 250–300 tons [21, 22]. In this way, using several devices to cover a wide range of runway state information at different conditions or developing new techniques to increase the friction coefficient measuring efficiency is necessary to reduce costs due to chemical rational dispensing, not to mention the environmental impact.

The frictional forces on the runway surface facilitate the ability to control vehicle direction and stopping distance, thereby minimizing collision risks. Operating conditions, tire characteristics, and pavement conditions collectively influence the tire-road interface. It is important to note that pavement property not only determine tire-road interaction but is influenced by these dynamic factors, emphasizing the multifaceted nature of pavement safety considerations [23].

The Federal Highway Administration has established a comprehensive pavement friction management program to mitigate friction-related vehicular accidents. This program includes four key priorities to ensure the achievement of its objectives. Firstly, it emphasizes the need to guarantee sufficient and long-lasting friction properties when designing and constructing new pavement surfaces. This measurement enhances vehicle traction and helps prevent accidents. Secondly, the program strives to identify and to address segments on the road that experience higher crash rates due to inadequate friction between the road surface and vehicles. Thirdly, it prioritizes allocating resources to implement cost-effective measures to reduce friction-related accidents. Lastly, the program emphasizes the importance of implementing effective data

collection and analysis methods for pavement friction, crash, and traffic data, aiming for accidents caused by insufficient road friction [24-30].

In a study conducted by Elkhazindar A. [31], a survey questionnaire was distributed to 42 state Department of Transportation representatives. These representatives, in turn, forwarded it to the relevant individuals responsible for various areas, such as research, materials, management, or design personnel, in the United States. This study's objective was to gain comprehensive insights into the official methods and strategies employed for managing pavement friction in the USA. These statistics addressed the existing conditions and practices related to state Department of Transportation (DOT). Based on the survey findings, state agencies' most common method to measure friction is the locked wheel testing practice. In addition, most state DOT policies need to adhere more to a standardized management system and establish clear maintenance targets and comprehensive plans. Nevertheless, most state DOT have implemented some level of Pavement Friction Management and related programs in various initiatives that vary from rudimentary and subjective approaches to sophisticated systems that involve regular testing, long-term planning, and extensive research dedicated to friction treatments [31].

Theoretically, the friction between a rubber tire and a road surface contains two distinct elements: adhesion and hysteresis. Adhesion refers to the shear force between the tire and the road surface as the tire conforms to the contact area. Initially, adhesion friction is predominant until a critical slip occurs. On the other hand, hysteresis deformation happens due to the dissipation of energy and damping losses in the tire's rubber. Thus, during sliding, the adhesive component decreases while hysteresis increases [32, 33].

Factors Affecting Friction

Friction is commonly represented by a dimensionless coefficient, generally denoted as μ, rather than being expressed directly as a force (see, Figure 4). This coefficient, known as the friction coefficient, is determined by dividing the total frictional force (F_{f}) acting on an interface by the total vertical load or normal force (F_N) applied to the same interface [34-36].

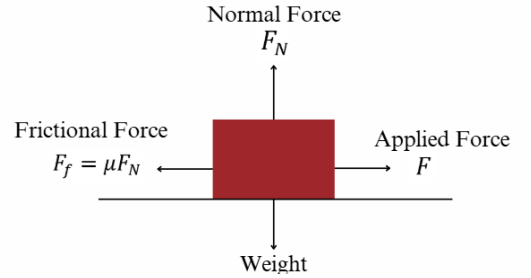

Figure 4: Coefficient of friction forces diagram.

$$\mu = \frac{F_f}{F_N} \qquad (1)$$

Multiple variables influence the friction generated during aircraft operations. These factors encompass the aircraft's speed, total weight, the use of reversed engines thrust, crosswind intensity, pilot expertise, runway length, interfacial contaminants, and pavement properties. For proper taxiing, takeoff, and landing, each aircraft requires a specific level of friction to ensure sufficient deceleration and directional control stability [21]. The mechanics behind skid resistance are intricate, and the precision of its measurement is markedly affected by fluctuations in environmental factors [33].

Skid resistance measures the friction generated under specific, standardized conditions. These conditions are generally chosen to fix the values of many potential variable factors, with the aim of isolating the road's unique contribution to tire/runway friction [37, 38]. Airport authorities are crucial in maintaining the standards for airport pavement performance. Over time, the skid resistance of a typical lane on a pavement naturally decreases due to the repetitive traffic movement in a specific direction. The skid number varies at different locations on the runway due to factors such as vehicle speed and weight [11, 33, 39, 40].

Skid resistance parameters can be classified into four distinct categories: surface aggregate characteristics (texture, roughness, and material composition), load-related factors (wheel pressure and contact area), environmental conditions (temperature, moisture, and contaminants), and vehicle factors (tire tread design, inflation pressure, and speed). Among these classifications, surface aggregate factors can be controlled, while load factors can be regulated to a certain extent. However, when discussing pavement characteristics, the skid resistance properties are predominantly influenced by the microtexture and macro texture [41-44].

Figure 5 displays the key mechanisms of pavement friction: adhesion (microtexture) and hysteresis (macro texture). Microtexture, composed of individual stone texture, refers to the surfaces irregularities of the pavement that are challenging to perceive with the unaided eye, within a wavelength range smaller than 0.5 mm, encompassing textures up to 0.5 mm in depth (ISO 12473-1). Macro texture is linked to the texture that arises from the arrangement of individual stones, referring to the pavement irregularities that exist within a wavelength range spanning from 0.5 mm to 50 mm, encompassing textures deeper than 0.5 mm as defined by ISO 12473-1 [45].

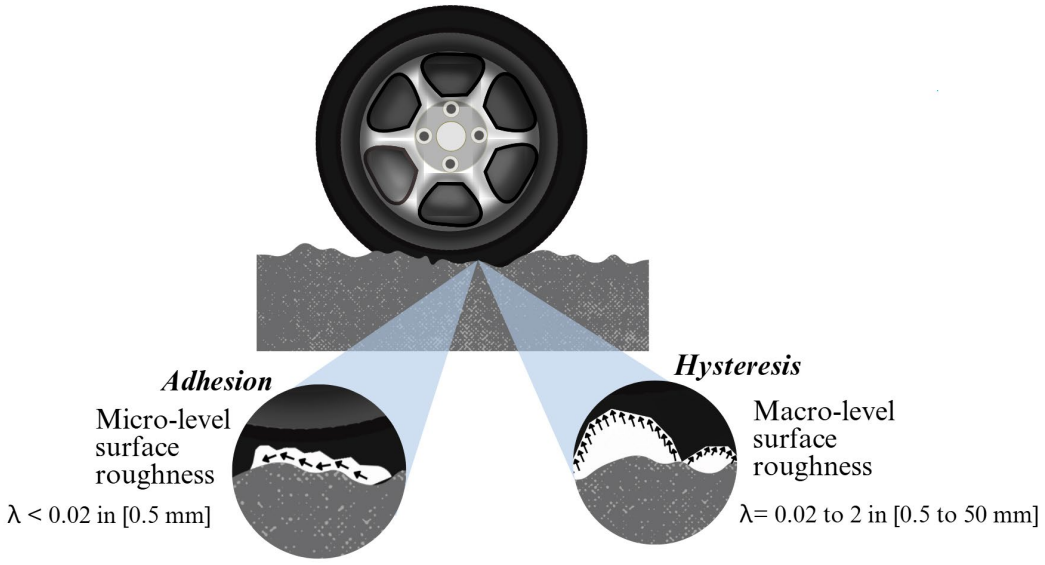

Figure 5: Key mechanisms of pavement-tire friction (λ= wavelength). Inspired on [24].

The adhesion force is influenced by the surface microtexture's wavelength and Mean Profile Depth (MPD). MPD is described as the difference between the highest point and the average height of the surface profile. The macro texture impacts the vehicle suspension system, energy dissipation, induce bending or flexing of tire sidewalls, and heat waste. During sliding, the hysteresis force acts when the rubber bends due to the aggregate particles present in the pavement's surface, causing the tire's energy dissipation as heat. In this way, adhesion and hysteresis, are highly dependent on the surface features, the interfacial surface of contact, and the tire properties [34, 46].

Rolling friction is primarily attributed to deformation losses in plastic materials and hysteresis losses in the elastic regime [47]. Since hysteresis friction arises from the interaction between tire rubber and pavement

macrotexture, with microtexture playing a supporting role, changes in friction behavior can provide insights into its contribution. Although the exact proportion of hysteresis friction cannot be determined solely from the friction coefficient, comparing different pavement conditions allows for an assessment of its relative influence. A decreasing friction coefficient indicates a reduction in hysteresis friction, reflecting variations in the energy dissipation mechanisms between the tire and the surface [48].

2.3 Measurement of Skid Resistance in Winter Conditions

Runway surfaces are exposed to a wide range of contaminants from different natures during winter, such as freezing drizzle, freezing rain, and hoar frost, or any of the ice mitigation materials currently available, such as liquids and solids chemical products for runway de-icing (road salt, potassium formate, potassium acetate, hybrid liquids). The contaminants affect the surface properties of the concrete and, thus, the skid resistance [49, 50].

Runways are generally divided into three main sections: the touchdown zone, the midpoint, and the rollout zone. During winter, runway inspectors routinely access the runway to gather vital data from each of these sections, referred to as ''runway sections''[51]. This data compilation encompasses essential details such as the nature of the contaminants, runway temperature, spatial coverage, and dew point temperature. For the assessment of braking parameters, ground friction measurement equipment is extensively employed to ascertain friction coefficients [52, 53].

Multiple testing methods enable worldwide airport operators to assess the runway's skid resistance under winter conditions. Table 1 provides an extensive inventory of these techniques, categorized on their principle, with the associated standard, measurement index, advantages, and limits.

The devices based on the longitudinal friction coefficient principle are recognized by the tires' sliding process control using the braking force system [11, 54]. Fixed Slip devices measure the friction experienced by vehicles with anti-lock brakes and maintain a constant slip, typically between 10 and 20 percent, as a vertical load is applied to the test tire [24]. The side-force method assesses the vehicle's ability to maintain control when maneuvering curves by measuring the side-force coefficient. This coefficient quantifies the capacity to uphold a steady angle known as the yaw angle between the tire and the direction of movement [24]. The slow-moving LFC principle uses rubber sliders, which slow down when in contact with the

pavement surface; thus, these devices are used in a laboratory and are stationary tests [11]. Finally, Decelerometers are devices that measure the deceleration of a vehicle while braking. They operate with the help of an inertial sensor called an accelerometer, which assesses deceleration by analyzing the braking slip ratio. This slip ratio is obtained by dividing the tire's angular velocity when torque is applied by its angular velocity when not undergoing braking [34].

Table 1: Friction measurement devices that operates under winter conditions.

Principle	Device	Standard	Measurement index	Advantages	Drawback
Longitudinal Friction Coefficient	IMAG	ASTM E1859	Due to the freely rotating wheel, the friction test can be performed under variable slip ratios. Therefore, the wheel speed, vehicle speed, travel distance, friction force, and upper loading will be recorded. Furthermore, this testing system can output the friction number, and the relation curve between the slip ratio and FN will eventually be obtained.	Continuous testing: Friction data can be acquired at any designated slip ratio. The shape factor from the Rado model can also be obtained from this test, facilitating further in-depth analysis.	Large scale testing facilities are usually required for this test, accompanied by high expenses in measurement and maintenance and time-consuming data processing. A high-capacity water tank is required for continuous long-distance measurement.
	RUNAR				
	SALTAR				
	Grip Tester	BS7941-2:2000	The test is usually performed under a given slip ratio, partially confining the tangential rotation of the test wheel. Thus, the wheel dragging force can be measured, together with the upper wheel load, for the calculation of FN in this pattern of testing report.	It is an economical management device, reliable, versatile, and easy to use.	Low normal force results in excessive loss of contact at highway speeds
	ROAR	ASTM E1551		It can operate at 20 km/h to 130 km/h, act as a stand-alone instrument, or be towed by a host vehicle.	The cost is significantly higher than that of other friction devices.
	Skiddometer BV-11	ASTM E1960-98		Continuous testing: Friction data of high resolution can be collected	The testing data is collected at a designated slip ratio, accounting for some difference between testing mode and actual braking condition, especially on a snowy or icy pavement surface. The high-capacity water tank is required for long-distance measurement.
Fixed Slip	RFT	ASTM E 1551			
	SFT				

Sideway Friction Coefficient	Mu-meter SCRIM	ASTM E 670	The ratio of the sideways force to the vertical force between the tire and the road surface.	The test can be conducted on complicated road alignments, such as curves and steep slopes. Continuous testing: widely used in Europe	Due to the distinct slip angle between the test wheel and the drive direction, pavement unevenness, such as potholes and cracks, can damage the test wheel.
Rotating Friction	DFT	ASTM E1911	Rubber pads on the rotating plate will contact the testing surface as the plate is motivated to reach the target speed. Afterward, the speed of the pads will be slowed down to zero owing to friction in the contacting interface, with the friction coefficient measured at a given speed.	This device can be used in lab and field testing. It is highly repeatable, reproducible, and unaffected by the operator's procedure or wind. This method's results produce friction coefficients that represent high-speed values.	There is still some distinct difference between DFT and actual tire-pavement frictional behaviors, triggering the accuracy reduction of DFT in estimating frictional coefficient in situ.
Transitional coefficient of friction	Mark IIIB	ASTM F2508	Measures the transitional coefficient of friction by simulating the biomechanical movement of a pedestrian	Test rapidly, with minimal operator error and easy collet repeatable measurements.	Disturb surface conditions to a lesser degree but over a larger area. Measurements take longer to execute and are highly impacted by the presence of salt particles.
Polishing Wehner/Schulze	Wehner /Schulze	EN 12697-49	As the test head decelerates, the friction value μ is recorded, and the friction value is reported as the μPWS.	It determines the friction dependency on speed and can be used to develop new materials and construction methodologies for a surface course.	The gap between the simulated work condition and the natural friction state.
Pendulum test	British Pendulum Tester	ASTM E303	Rubber sliders, attached either to the foot of a pendulum arm or to a rotating head, slow down on contact with the pavement surface. Thus, they are used in lab and stationary tests.	It can be used for both field and laboratory evaluation. This device is highly portable, easy to handle, and does not require surface preparation or external energy.	It needs traffic control and lone closure. Because of its spot measurement, it cannot be used for network evaluation. It only measures the frictional property of a surface at a low speed. BPN has a large variability, and operator procedures and wind can impact it. Measurements on snow and ice are criticized.

Slow-moving Longitudinal Friction Coefficient	T2GO	EN 1436		—Allows continuous measuring of the skid resistance at low speeds. —Can measure friction on both dry and contaminated surfaces. —Manual and portable roughness tester.	—Mainly for road marking testing. —A device pushed by hand. —Challenging to calibrate it. —It may provide results with significant variations, resulting in an inaccurate estimation of the surface slipping risks.
	VTI BV14	ASTM E1960-98		Especially developed for winter	Not able to measure wet friction
DEC	TES MK 3	AC 302-026	Travelling at standard speed (32 to 48 km/hr), the brakes lock the wheels until deceleration rates can be measured. The deceleration rate is recorded for friction computation.	—Convenient and simple to operate. —Simple installation and removal. —Low maintenance design.	Poor correlation with actual aircraft stopping performance in wet and flooded pavement conditions.
	Bowmonk ERD	ISO/IEC 17025		Simplicity	Longer runway occupancy time
	James Brake	[i]		Instantaneous deceleration reading.	Must be reset between each reading
	Tapley meters	[i]		Simple to operate, needs very little operator training, low maintenance costs	Traffic interference

[i] information not available

Laboratory Testing Methods

The primary approach for assessing the skid resistance of pavements and runways entails examining their microtexture [8]. For assessing low-speed pavement skid resistance, the British Pendulum Tester (BPT) and Dynamic Friction Tester (DFT) emerged as the two most frequently employed instruments [55].

The BPT, a test developed in the 1950s by the UK Road Research Laboratory, is a reliable method for measuring the skid resistance of road surfaces [56]. Operating on the Charpy test principle as shown in

Figure 6, this dynamic evaluation method uses a rubber slider in contact with the surface to assess skid resistance. The BPT test, widely used in laboratory settings and friction testing, provides a result in the form of the British Pendulum Number (BPN). A higher BPN value indicates a surface less likely to slide, serving as a proxy measure of the pavement surface's micro-texture quality and its contribution to skid resistance [56].

Figure 6: British Pendulum Tester at the Anti-Icing Materials International Laboratory.

Brassard et al. [8] utilized the BPT to establish a relationship with the Global Reporting Format. Canada implemented it in 2021 to mitigate hazards and risks associated with operations on contaminated runways with frozen precipitation. In their article, they presented a comprehensive testing method for liquid runway de-icing products, with direct implications for the aviation industry.

Throughout their research, they observed how surface conditions were affected, comparing untreated surfaces to those treated with liquid runway de-icing products in both de-icing and anti-icing modes. The outcomes obtained from the British Pendulum Tester on concrete strongly correlated with the Runway Condition Code ratings [8].

However, is important to mention that according to ASTM E303-22, the BPT was only designed to operate on dry and wet flooring conditions [57].

On the other hand, the DFT, as illustrated in Figure 7, is a highly versatile instrument. It can measure the frictional properties of pavement under various speeds, with a particular emphasis on high speeds. This adaptability makes it invaluable for acquiring data on tire-pavement frictional behaviors. The

equipment, with its distinctive rectangular design, features a disk on its lower side with three rubber pads attached. The disk is powered by a DC electric motor to perform measurements, propelling it to reach a target circumferential speed set by the operator using the control unit. When the rubber pads achieve the predetermined speed, the electric motor is deactivated, and the disk, along with the measurement pads, is lowered onto the pavement surface under a consistent vertical load. The friction engendered by the contact between the pads and the surface gradually reduces the pads' speed until they come to a complete halt [58, 59].

DFT is suitable for assessing pavement friction in both field and lab tests. However, lab tests present a challenge due to the need for larger specimen sizes to accommodate the DFT testing area, leading to the use of specialized molds and handheld compactors for slab preparation. As a result, the DFT is more commonly utilized in field tests. However, practical lab tests can also be conducted by adopting a combined pavement core drilling in situ technique if strict control over height deviation is ensured [58, 60].

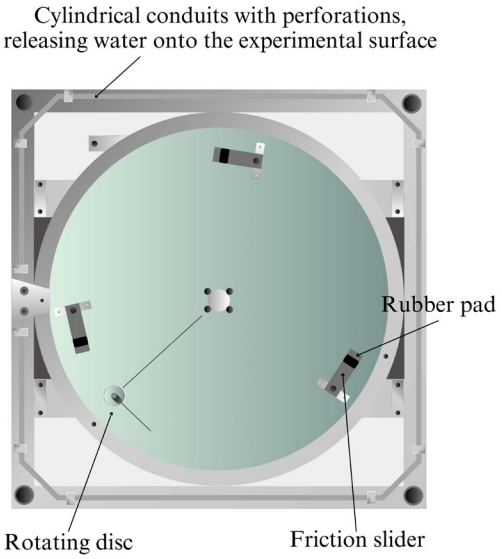

Figure 7: Dynamic Friction Tester representation (bottom view).

Tan et al. [61] used the DFT to quantify the skid resistance of asphalt pavement under icy conditions (four different types of ice thickness). This study evaluated the dependency of friction coefficients on velocity and ambient air temperature. In summary, their findings indicated that the device could be utilized to examine icy tracks, offering a valuable tool for studying the interaction between tires and ice in tribological investigations. However, they have yet to explore the impact of snow using this device.

The Wehner/Schulze device was developed in Germany in the 1960s and primarily intended to analyze asphalt mixes using rolling friction by a wheeled mechanism of three rubber heads for polishing the surface sample and a separate measuring head equipped to assess skid resistance [62]. This device's ability to simulate both the polishing and measuring of skid resistance on flat, circular specimens have allowed it to be applied to studying various surfaces, including aggregates and actual road surface layers from field cores or lab-produced samples [62]. Over recent years, the Wehner/Schulze device has been increasingly utilized in research to investigate skid resistance in aggregates and surface layers. Additionally, it has been essential for establishing correlations between lab-based measurements and real-world field measurements [41, 63].

Wang et al. [50] measured the skid resistance of different gritting materials, including de-icing products using the Wehner/Schulze device at 60 km/h aiming to align with the Sideways-force Coefficient Routine Investigation Machine (SCRIM) measuring speed, and in this way determine the effect of the road treatments used in winter maintenance practises imitating real-life scenarios. They simulated polishing using the Aachen Polishing Device (APD) and adjusted winter products' size and shape, such as de-icing salt, quartz sand, and quartz powder. The results of this study displayed a change in the skid resistance because of the de-icing agents. They indicated de-icing product as an ideal option compared to the other agents for its effect on the skid resistance performance during winter to improve traffic safety [50].

The T2GO is an innovative, low-weight testing instrument with two test rubber wheels to evaluate friction on dry and contaminated surfaces. It operates at a test speed of 1 m/s, providing precise data at intervals of 0.1 meters. This device analyzes skid resistance. In contrast to conventional devices that typically operate at approximately 60 km/h speeds, the T2GO functions at a slower walking speed [48, 64]. One of the key advantages of the T2GO is its ability to control the tire slip rate at 20%, which proves especially beneficial for accurately measuring the friction coefficient on pavements covered with snow and ice. This capability sets it apart from other testing instruments and makes it a valuable tool for assessing road conditions in winter weather [48].

In research conducted by Li et al. [48], the T2GO tester assessed the pavement friction coefficient within a temperature range of -5 °C to -6 °C. The study aimed to replicate the road surface conditions

experienced during harsh winter weather in an advanced cold chamber. By analyzing the deterioration mechanism of the friction coefficient, the study identified critical indicators related to ice and snow contamination, which influence the skid resistance of pavements. Interestingly, the results revealed distinct mechanisms through which the ice and snow layers affect the attenuation of pavement skid resistance [48].

Mark IIIB is a tribometer from the United States that replicates the biomechanical motion of a pedestrian slipping on a surface. To conduct the test, the device repeatedly modifies the angle between a rubber test foot and the pavement surface until the test foot slips upon being launched from the device [65].

SlipAlert, a tribometer hailing from the United Kingdom, imitates the sliding movement of a vehicle. This device comprises a miniature model car with a rubber slider on its underside. To operate it, the distance the car covers over the pavement surface is recorded after launching it down a ramp [65].

Marvin et al. [66] researched the effects of Mark IIIB and SlipAlert's devices on Permeable Interlocking Concrete Pavement (PICP) in winter conditions. The aim was to establish best management practices for winter operations in cold climates. The study found these devices suitable for winter measurements but noted that they altered surface conditions when snow and slush were present. This made test repeatability challenging, as the surface became unusable after one test. Mark IIIB's method caused compaction and heat transfer, requiring accurate angle estimation to minimize disruptions. SlipAlert, however, collected friction measurements with a single car launch, causing less disturbance but covering a larger area due to its longer sliding path. Thus, Mark IIIB allowed the estimation of less common transitional friction measurements and demonstrated the capability to collect spot measurements on isolated patches of ice and snow. In contrast, SlipAlert, does not require multiple measurements, is less impacted by the presence of salt particles, and less time consuming [66].

The array of friction-measurement instrumentation accessible globally exhibits substantial diversity. Nevertheless, infield apparatuses constitute a significantly larger domain, encompassing varied configurations meticulously designed to align with the specific requisites of distinct sectors, countries, or scenarios.

In-Field Testing Methods

Numerous techniques have been devised to monitor the state of runway surfaces and appraise their braking performance. Many of these techniques are based on ASTM test methods that assess the surface friction characteristics [39, 57]. The most used tests involve fixed devices that enable direct measurement of the friction between the runway and the tire. These apparatuses can conduct various tests, such as the lateral force test (ASTM E670), fixed slip test (ASTM E2340), and locked wheel test (ASTM E274) (Table 1) [8, 67-69].

Norsemeter Holding ASA from Norway developed the Road Analyzer and Recorder (ROAR) and the Runway Analyzer Recorder (RUNAR) units to measure pavement friction and surface characteristics of road and airport runways, respectively. The Salt Analyzer and Recorder (SALTAR) device, another Norsemeter system, was also designed as a friction tester for Salt trucks [70].

The Joint Winter Runway Friction Measurement Program (JWRFMP) carried out various tests under bare and wet, slush, loose snow, smooth and rough ice, and mediums and hard-packed snow, in the Jack Garland Airport, located in North Bay, Ontario, Canada, using different friction devices, such as Grip Tester, RUNAR, and Surface Friction Tester (SFT). As a result of this study, different findings were concluded.

First, the correlation between friction devices on wet pavements does not hold for ice—or snow-covered pavements. This implies that pavements covered in ice and snow exhibit dissimilar characteristics compared to wet pavements, having almost doubled the average critical slip value on ice and snow.

Secondly, as part of the JWRFMP, the SALTAR unit was also tested in Canada under extreme cold conditions (-30 °C). The findings indicated that enhancements are needed to winterize this device. The freezing of the water in the lines reduced normal load on the test tire. Another important finding was that the friction values obtained from SALTAR measurements under the same conditions were notably lower when compared to those recorded by the reference device [70].

On the other hand, tests made by the National Aeronautics and Space Administration (NASA) runway friction workshop showed that SALTAR computation appears to be somewhat speed sensitive. Consequently, this device can provide accurate friction measurements when encountering low friction and

low speeds, considering that it was developed for the speeds of snowplows/spreader trucks that move at 50 km/h [70].

While numerous airports offer friction measurements during snowy or icy runway conditions, a significant concern arises from the need for more international standardization. In Norway, the commonly used devices are the Grip Tester and BV-11. The Grip Tester is easy to use and can measure up to 100 km/h, with just one operator needed for a runway survey. In contrast, France relies on the IMAG. This automatic skid resistance measurement device for runways continuously records the longitudinal, braking torque, and dynamic load on the wheel at a constant speed, ranging from 30 km/h to 100 km/h. IMAG, as shown in Figure 8, is employed to measure friction at various French airports, including Metz-Nancy-Lorraine, Orly, Roissy-Charles de Gaulle, Strasbourg, and Europort Vatry [22, 70-73].

Figure 8: Automatic Slip Measurement Instrument (IMAG) [74] © Richard METZGER / DGAC — STAC.

In 2008, the FAA introduced guidelines for measuring runway friction in winter (advisory circular 150/5200-30 C). They outlined two main tools: Continuous Friction Measuring Equipment (CFME) and decelerometers (DEC). The Mu-meter, Skiddometer BV11, and IMAG are advanced and most common devices in the CFME category. The Mu-Meter, a compact three-wheeled trailer crafted and produced in England, is a widely trusted tool. It can be towed by a vehicle or integrated into one, and features two tester wheels that measure sideways friction, typically at a speed of 65 km/h. The Mu-meter is not only used on airport runways, but its system is also adequate for work equally well on road pavements. Some tests have

shown that the Mu-meter device exhibited sensitivity to the influence of the macro texture on friction, achieved through a combination of drainage to eliminate water from the tire/surface contact and hysteresis losses. However, further research must be conducted to clarify those results [22, 75-77].

The FAA and the NASA Runway Friction Program conducted over 1000 tests with friction devices such as SFT, Mu-Meter, and the BV-11 Skiddometer. For the compacted snow and ice-covered conditions, all testing methods subjected to testing exhibited reliable and consistent readings. Furthermore, when comparing friction measurements between the SFT and the BV-11 devices, they were higher than the readings obtained from the Mu-meter and the SFT [70].

Figure 9 shows the Skiddometer BV-11, a continual friction measuring equipment developed by Moventor Oy, an international company specializing in friction measurement. The primary objective of this equipment is to facilitate secure friction measurement, even in the most challenging weather conditions, all without the need for batteries or complicated hydraulic or pneumatic systems that might easily break or malfunction. The Skiddometer CFME system can be provided with sensors to detect surface contaminants and temperature. This device allows airport operators to obtain precise information about the runway conditions for scheduling maintenance, such as snow and ice removal [78, 79].

Figure 9: Skiddometer BV-11 [79]. © Moventor Oy, 2024

One more significant device to consider in this section is the Sideways Force Coefficient Routine Investigation Machine. This device can detect road segments that meet or fall below investigatory thresholds defined for specific road categories. A survey conducted by SCRIM can be carried out at two distinct target test speeds: 50 and 80 km/hr. During this survey, skidding resistance data is consistently recorded by SCRIM and stored as an average value for every 5, 10, and 20 m segment of the road [73].

The DEC, a vital component in in-situ testing methods, employing braking to calculate the deceleration rate for friction determination. While these devices are not suitable for wet pavement and cannot perform continual friction measurements, they are the preferred choice for airports that cannot afford to extend runway closures for friction surveys or busy airports with limited access to full runways due to runway intersections. The TES Instruments Mk 3 Electronic Decelerometer (Figure 10), an approved device, is widely used in various airports across Canada and the USA for evaluating winter runway friction. Transport Canada has approved four decelerometers for use in Canadian airports, while five meet FAA technical specifications for the USA airport operations in wintertime [34, 80-82].

Figure 10: TES Instruments Mk 3 electronic decelerometer [81]. © TES Instruments, 2024.

Finally, the Bowmonk Electronic Recording Decelerometer is another essential device. Also known as the TC Electronic Recording Decelerometer, abbreviated as TES ERD, it utilizes a piezo-resistive accelerometer for measuring deceleration. Data is acquired by progressively applying the brakes until lockup is reached, followed by their release. This device is recommended exclusively on runway surfaces that are icy or have tightly compacted snow. The TES ERD was utilized in developing the Canada Runway Friction Index, a tool designed to measure runway slipperiness [83, 84] objectively.

Friction Data Interpretation

The interpretation, comparison, and analysis of friction values among studies pose significant challenges due to the multifaceted nature of the variables at play. Friction results not only depend on the specific device used but are also influenced by factors such as the thickness of the contaminant applied and the speed at which the tests are conducted. The interplay of these factors further complicates the ability to

draw meaningful conclusions from the data. It is worth noting that many studies need to include more critical information related to these variables, leaving a gap in our understanding of the results.

Table 2 displays the diversity of findings to enhance research transparency. It summarizes friction values obtained from the devices mentioned earlier and describes the conditions under which the studies were conducted. These conditions encompass an array of factors, predominantly the characteristics of the surfaces involved and the type of contaminants present during the testing. This comprehensive data set enables a more complete and informed assessment of the various studies and their implications.

Table 2: Friction values of various measurement devices under different conditions

Device	Condition or specification	Friction value	Ref
IMAG	Dry	0.7 - 0.9	[10]
	Smooth ice	0.1	
SFT	Dry, bare surface	0.8–1.0	[10]
	Wet bare	0.7–0.8	
	Packed snow	0.20–0.30	
	Loose snow/slush	0.20–0.50	
	Black ice	0.15–0.30	
	Loose snow on black ice	0.15–0.25	
	Very slippery ice	0.05–0.10	
Mu-meter	65 km/h	0.42	[85]
	95 km/h	0.26	
Speedometer	65 km/h	0.5	[85]
	95 km/h	0.34	
RUNAR	65 km/h	0.45	[85]
	95 km/h	0.32	
Grip Tester	65 km/h	0.43	[85]
	95 km/h	0.24	
BPT	Dry	50 BPN	[8]
	wet with water	38 BPN	
	Removed snow	33 BPN	
	Snow	23 BPN	
	Wet snow	19 BPN	
	Ice	17 BPN	
	Snow on ice	11 BPN	
SALTAR	Good	>0.5	[86]
	Acceptable	0.4 — 0.5	

	Slippery	0.25 — 0.4	
	Very slippery	0.15 — 0.25	
	Hazardous	<0.15	
ROAR	Bare and dry	0.8	[86]
	Bare and wet	0.7	
	Slush	0.4	
	Wet ice	0.1	
Runway Friction Tester	65 km/h	0.5	[85]
	95 km/h	0.41	
DFT	Dry	1	[61]
	Wet	0.5	
	Natural snow	0.6	
	Compacted snow	0.58	
	Icy	0.12	
T2Go	Dry pavement	1.26	[48]
	A layer of thick ice	0.173	
	Snow layer	0.43 - 0.45	
TES MK3	Dry	1 CRFI	[82, 87]
	Dry snow on the pavement	0.16 — 0.76 CRFI	
Bowmonk ERD	Dry snow on ice	0.12 — 0.25 CRFI	
	Sanded packed snow	0.23 — 0.47 CRFI	
James Brake	Bare-packed snow	0.12 — 0.31 CRFI	
	Sanded ice	0.19 — 0.35 CRFI	
Tapley meters	Bare ice	0.07 — 0.22 CRFI	

Most friction measurement devices typically provide results ranging from 0 to 1, where 1 represents dry conditions, and 0 means slipperiness, representing a continuum of friction values. However, there are exceptions, such as the BPT, which yields results in BPN. The BPT results strongly correlate with the GRF rating system [8, 88].

The ideal runway condition for aircraft operations is a dry surface. This corresponds to a top RWYCC score (6) and high BPN (50 ± 3). It ensures excellent friction and minimal skidding risk, thus making it the safest runway scenario [8].

Conversely, when snow is added to the icy surface, the BPN value drops significantly to approximately 11 ± 2. This corresponds to an RWYCC of 0, indicating the worst possible runway condition. The runway

poses the highest risk in this state due to highly reduced skid resistance, making it hazardous for aircraft operations [8].

To make a direct comparison between devices, it is necessary to select specific parameters, such as interfacial conditions. These parameters are not just for simplifying the correlation of the methodologies, but also to guide your understanding of the results. For instance, the variability in wet conditions can be substantial, contingent upon factors like temperature and ice or snow on the runway under wetting conditions. Therefore, Table 3 is a guideline to comprehend diverse values across three surface conditions. It is crucial to underscore that these values are derived from the outcomes of various tests, wherein distinct experimental features and specificities directly influence their magnitude.

Table 3: Friction coefficients for runway surfaces under different contaminants: dry, wet, and ice conditions [8, 10, 85, 89].

Condition / Apparatus	IMAG	SFT	BPT	ROAR	DFT	T2Go	Decelerometers
Dry	0.7 - 0.9	0.8–1.0	50 BPN	0.8	1	1.26	1 CRFI
Wet	0.2-0.8	0.7–0.8	38 BPN	0.7	0.5	0.25-0.4	0.2-0.3 CRFI
Icy	0.1	0.15–0.30	17 BPN	0.1	0.12	0.173	0.07 — 0.22 CRFI

Furthermore, the last column featuring DECs mentions TES MK3, Bowmonk ERD, James Brake, and Tapley meters. Transport Canada has strategically opted for a standardized methodology, choosing these particular DECs for evaluating runway friction on surfaces affected by winter conditions. This decision stands out given the extensive range of devices available in the market, each designed to measure the runway surface friction [82].

Furthermore, it is essential to emphasize that Transport Canada relies on the Canadian Runway Friction Index (CRFI) to quantify the average runway friction measured by a DEC on runways affected by freezing or frozen precipitation. This index provides friction values from 0 to 1, 1 representing a vehicle's theoretical maximum deceleration capability on a dry surface. This index is a critical metric for evaluating runway conditions, especially in challenging weather circumstances. Notably, the CRFIs used in landing distance tables are primarily based on friction measurements gathered using DEC [82].

Comparison Between Laboratory and Field-Testing Methods

Vehicles or instruments equipped with friction measurement capabilities can evaluate pavements' skid resistance in actual field conditions (in situ) or controlled laboratory environments (lab). Notably, a more extensive array of techniques is accessible for field assessments than for laboratory environment [33, 90].

Some studies have found that the Wehner/Schulze device for lab testing has replaced the BPT thanks to the speed range and pavement specimen size. This is significant because it allows quicker and more efficient testing, particularly in high-volume testing scenarios [63, 91-93]. On the other hand, Al-Qadi et al. [70] showed during their studies that SALTAR tends to provide lower friction coefficients than the ROAR for the same iced surface conditions. However, the friction values behave the same, increasing and decreasing proportionally. This finding is important as it suggests that while the absolute values may differ, the relative performance of the surfaces remains consistent. Finally, their data indicated that devices of variable slip, such as IMAG, RUNAR, and SALTAR, and the deceleration devices, such as TES MK 3, could potentially provide the most suitable approaches for measuring friction in winter conditions because of their cost efficiency, data accuracy, portability, and ability to conduct repeatable friction measurements. This conclusion is valuable as it provides a practical solution for winter friction testing [70].

The ASFTs, whether mounted on a vehicle or hauled by a trailer, are fully part of the ASTM standard tests for infield friction measurement. They are widely used and continuously evolving, making them the most popular method for measuring runway friction [94]. In contrast, for laboratory testing, the BPT has been established as a standard laboratory test for evaluating the friction properties of pavement surface materials, thanks to its good reproducibility, low cost, lightweight, and well-established standardized test procedures [56].

Test continuity is essential for airport operators to obtain continuous pavement skid resistance and determine the runway maintenance threshold. CFMEs are commonly found to measure the friction performance of airport pavement. There are many continuous in-situ measurement methods compared to lab testing techniques. One such hybrid device is the T2Go, which can be used in the lab and field, providing a comprehensive assessment of pavement conditions in both environments. This emphasis on continuous

in-situ measurement methods should reassure airport operators about the accuracy and reliability of their runway maintenance decisions [95].

Infield testing typically requires additional equipment, such as the Griptester MK2, BV11, and ASFT T-10, which requires constant feeding of water from a vehicle's tank, making it time-consuming. However, infield equipment allows for testing under real-world conditions, ensuring greater representativity and providing more accurate and relevant results. This limitation for infield equipment is a strength of laboratory devices since devices such as BPT are portable and do not need surface preparation or external energy to test. This makes them more versatile and easier to use, but their results may sometimes not be representative enough [8].

2.4 Conclusion

This chapter has thoroughly examined the various methods and equipment used to evaluate the skid resistance of runway surfaces under winter conditions, a pivotal aspect of aviation safety. We started sharing the historical roots of the tribology field, showing the different components that build it, followed by the pavement friction and the factors that affect its response, discussing essential terms such as micro and macro texture to introduce the measurement of skid resistance under winter conditions with an extensive table that classifies the current existing devices to measure friction under these conditions. From this table, we then found different research studies that provided insights into the performance of those devices. Ultimately, we compared the results we can obtain with the friction devices for a specific winter condition.

The most commonly used in-field devices include the Grip Tester, Mu-Meter, and the IMAG, which is particularly popular in Europe, along with decelerometers. Multiple testing devices and techniques, including the BPT, DFT, and CFME like the Mu-Meter and Skiddometer BV-11, have been analyzed for their effectiveness in both laboratory and field settings.

The importance of selecting friction measurement tools tailored to specific environmental and operational contexts is evident from the literature review. Devices like the T2GO and DEC are particularly effective due to their portability and accuracy on snowy and icy surfaces.

Most friction measurement devices operate on a scale of 0 to 1, with 1 denoting dry condition and 0 meaning slippery and hazardous surfaces. However, devices such as the BPT, which generates readings in

BPN, and the Wehner/Schulze device, which reports in Wehner/Schulze Polishing (PWS) units, pose challenges for direct comparison and alignment with standardized normative values.

Given the lack of specialized laboratory equipment specifically designed for the aviation field, we are currently using alternatives like T2GO, Mark IIIB, and BPT, designed for pedestrian flooring inspections. While their portability and lightweight design are advantageous in laboratory setups, these devices were designed for less complex scenarios and do not consider the diverse variables found on runways, such as tire interactions, varying surface textures, and the presence of contaminants. Additionally, according to regulation, the BPT can only be used on dry and wet surfaces. Because of these limitations, developing a more suitable method became necessary to accurately assess aircraft runway friction.

Chapter 3: Experimental Development and Procedure

3.1 Introduction

The Multi-Tool Apparatus (MTA) was initially developed by Brassard et al [96] for measuring ice adhesion with an ice scraper attachment simulating the human motion to remove ice from covered surfaces. To address critical gaps in current friction laboratory methods in aviation, the MTA was adapted to measure friction. While decelerometers provide standardized field measurements for winter runway maintenance as part of the GRF, there is a lack of specialized laboratory devices capable of reproducing representative winter conditions meeting the standards and measuring friction in winter conditions.

Existing tools, such as the British Pendulum, were developed for floor inspections, and do struggle to operate in complex winter conditions such as snow and slush. BPN unit is difficult to correlate with field data and standards. The MTA was specifically tailored to meet these needs by simulating the interaction between aircraft wheels and runway surfaces using varying speeds and normal loads.

This chapter presents the MTA characterization, the friction tests with their respective parameters and conditions, a description of the cold chamber used for the precipitation experiments, the 3D profilometry setup, and the Runway De-icing Products (RDP) testing methodology. By reviewing this chapter, the reader is expected to gain a clear understanding of the essential features of the testing processes.

3.2 Components and methods

MTA characterization

The primary objective of this study is to investigate the potential of the MTA device to simulate the interaction between aircraft wheels and a runway contaminated by icing precipitation. The device measures friction at controlled velocities ranging from 0.5 mm/sec to 74.0 mm/sec, using a rounded rubber attachment (see Figure 11). While this speed range is significantly lower than typical aircraft speeds during landing or takeoff, it is suitable for controlled friction measurements in a laboratory setting. The MTA uses a double-acting pneumatic cylinder with adjustable pressure settings to precisely measure the maximum force, in

Newton, required to move the rubber at a predefined speed. All experimentally acquired forces are instantly transmitted and recorded in real time in a Excel™ file through LabVIEW™ interface.

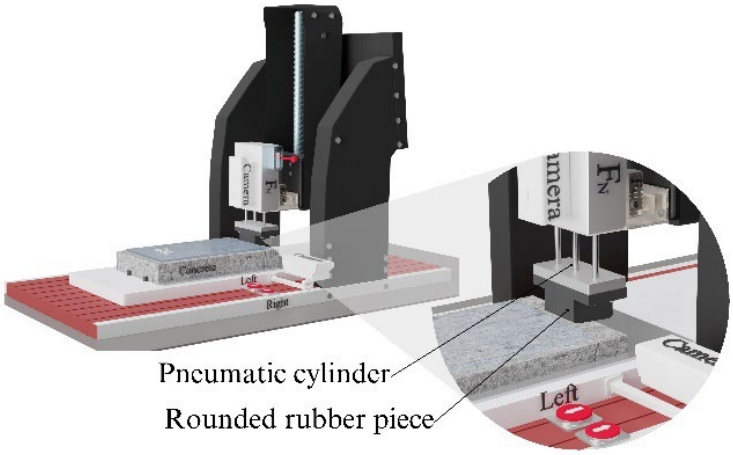

Figure 11: Multi-tool apparatus close-up with parts.

The unit is integrated into a four-axis machining system with controlled motions and features dual cameras for inspecting rubber passage. The apparatus accommodates normal forces (FN), ranging from 0 to 56 N, allowing for precise control over the applied load during experiments using compressed air. This range was chosen based on previous studies and represents an applied weight of approximately 5.7 kg. The apparatus can handle substantial forces, with a maximum capacity of 200 N, ensuring it can evaluate materials' friction performance under significant outdoor conditions. Forces are recorded through an interface developed with LabVIEW software at a rate of 1000 Hz, with the load cell placed over the scraper. Operating within a temperature range of −30 to 20 °C, it effectively simulates tire-runway interaction in cold climate conditions, enabling comprehensive testing of friction.

MTA Calibration

As an initial step in characterizing the MTA, a calibration test of the load cell is performed to determine the relationship between the applied force and the corresponding voltage output. This relationship allows the load cell to accurately measure tensile forces during experimental procedures. The calibration process follows a systematic methodology to ensure precision and reliability.

Firstly, the mechanical stability of the load cell is verified before calibration. This is achieved by subjecting the load cell to a steady load of 54.23 N for 24 hours, ensuring that the sensor reaches a stable and reliable state.

Once the load cell is mechanically stable, the calibration process begins. A known force is applied to the load cell, and the resulting voltage output is recorded. Each known force value corresponds to a specific voltage reading, and this process is repeated across a range of force values by applying loads from 0.1 to 1.7 kg. The relationship between force and voltage is expected to be linear, meaning that the voltage increases proportionally with the applied force.

By plotting the force versus voltage data, a linear relationship is established, allowing for the determination of the constants (slope and intercept) of the calibration curve. These constants are unique to each load cell and enable accurate analogical conversion of voltage readings into force measurements during actual tests.

Secondly, to optimize the performance of the MTA system, it was crucial to thoroughly understand its operational mechanics, particularly how it behaves at different velocities. To achieve this, a dedicated test was conducted to analyze the machine's speed response under varying frequency settings.

This test involved running the MTA at 17 different frequency values, ranging from 1 Hz to 150 Hz, to cover a broad spectrum of potential operational conditions. A GoPro camera, was strategically positioned to capture the exact moment the machine passed two designated reference points. One video was acquired for each test iteration. By recording the time, it took for the machine to travel between these points, we could accurately determine its velocity.

This approach provided a precise and reliable measurement of the machine's speed at each frequency setting, offering valuable insights into how the MTA behaves under different velocity conditions.

MTA Friction Tests

The MTA was implemented to evaluate friction levels on concrete surfaces under controlled winter conditions. Testing was conducted in one of the AMIL cold chambers of the Université du Québec à

Chicoutimi, replicating the most common GRF surface conditions reported by the Montreal and Paris airports: dry, wet with water, snow, removed snow, and ice [8].

A total of 310 friction tests were conducted using ten standard concrete specimens. To ensure clarity and proper understanding, the testing plan was divided into velocity and normal force. The protocol began with velocity tests performed under dry and icy conditions to determine the optimal velocity at which the MTA operated with minimal induced error. Subsequently, normal force tests were conducted first under dry, wet, and icy conditions to assess the effect of the normal load on the device's friction response. Based on these results, the optimal normal force was selected to carry out the remaining tests, which incorporated surface treatments for both de-icing and anti-icing modes. The tests were conducted according to the following specifications:

Velocity Tests

In this part 80 tests were conducted to analyze the effects of varying velocities on friction under controlled temperature conditions. The tests were evenly divided, with half performed under dry conditions (RWYCC 6), serving as a reference value without any treatment, and the other half under ice conditions (RWYCC 1).

The ice condition was created by simulating freezing drizzle for 30 minutes using Nozzle #11001, which has a mean volumetric diameter of approximately 320 µm and produces an ice thickness rate of 5 to 8 mm per hour. This rate aligns with typical freezing drizzle events observed in airport environments. The resulting ice resembled glaze ice, commonly formed under supercooled drizzle conditions [96].

During this phase of the experiment, the normal force was kept constant at 226 N, the maximum load the machine can apply. This ensures stable and consistent contact, minimizing surface texture effects. A higher load increases the real contact area, enhancing adhesion, while also maintaining cohesion within the rubber attachment, leading to more reliable friction measurements. Friction measurements were taken at four different velocities: 0.004 m/s, 0.007 m/s, 0.028 m/s, and 0.049 m/s. This range of velocity provided valuable insights into how friction levels varied with velocity, enabling the selection of the optimal velocity for MTA operation.

Normal Force Tests

For the normal load test, the velocity was kept constant at 0.007 m/s, as velocity tests indicated that this speed level provided the most stable operation of the MTA, reflecting less variability across different tests. This choice allowed for a more precise assessment of the normal force's influence on the friction coefficient. For dry and wet conditions, the temperature was maintained at 20°C, while for the remaining conditions, it was set to -5°C. The five simulated conditions evaluated in this section are described in the following figure:

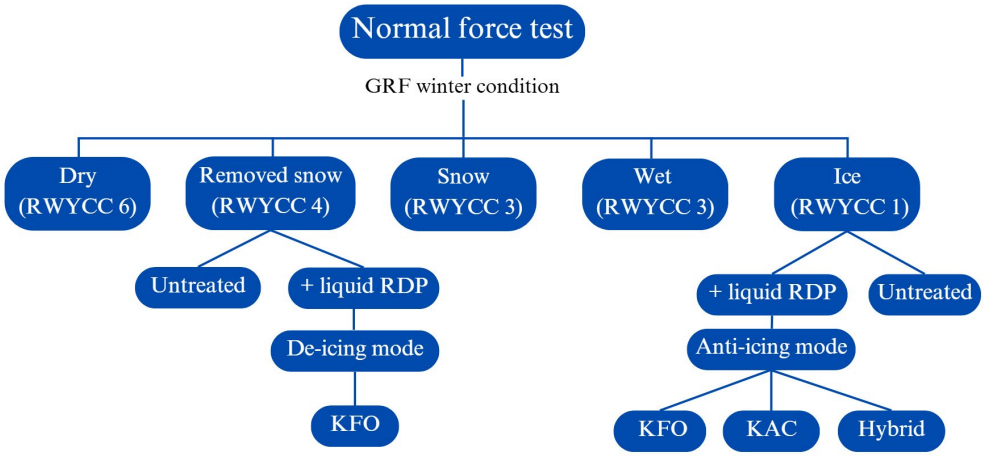

Figure 12: Normal Force validation tests plan using the GRF conditions.

After getting the reference values in the dry condition the following precipitation was the removed snow, which correspond to an RWYCC of 4. For this condition, as shown in figure 13 the snow was first sifted and pressed at low pressure, allowing it to fully fill the concrete's pores and after that an ice scraper was used to create the removed snow effect.

Figure 13: Removed snow condition with standard concrete sample (RWYCC 4)

For the snow condition, designated as an RWYCC of 3, a uniform layer of dry snow was applied to the interfacial surface of the concrete specimen. Unlike the removed snow condition, the snow in this test was not compacted, making it easy to remove, as you can see in figure 14.

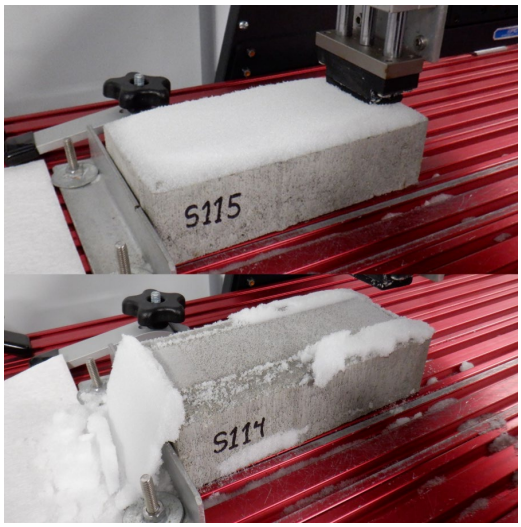

Figure 14: Snow condition before (top photo) and after (bottom photo) the test

In the case of wet condition, which is also part of the RWYCC of 3, the concrete sample was saturated with water following ASTM E303 specifications, maintaining the same room temperature as the dry condition [97] (see figure 15).

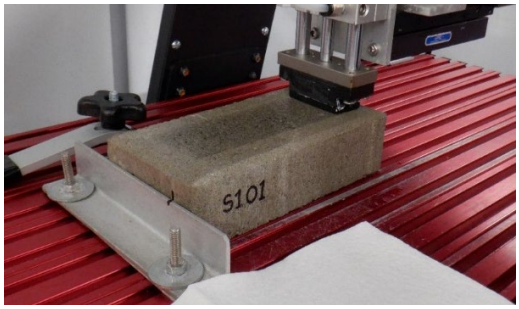

Figure 15: Wet with water condition with standard concrete sample (RWYCC 3)

Lastly, for the ice condition with an RWYCC of 1, the simulated conditions for the untreated samples were created using the same procedure outlined in the velocity test section.

Runway De-icing Products Tests

We also tested the MTA's ability to measure friction with liquid Runway De-icing Products (RDPs), evaluating their performance in both de-icing and anti-icing modes. Three widely used de-icing liquids were

selected and prepared at the Anti-Icing Materials International Laboratory using deionized water and commercial-grade salts to ensure consistent quality (see Figure 16). The tested RDPs were:

- RDP 1 (KFO, HCOOK): Formed of 50 % weight by weight Potassium Formate, with a freezing point of approximately -60 °C at this dilution.
- RDP 2 (KAC, CH_3COOK): Constituted of 50% weight by weight Potassium Acetate, also with a freezing point close to -60 °C at this dilution.
- RDP 3 (PG, $C_3H_8O_2$): The third product consisted of a hybrid RDP with an initial freezing point around -48 °C. Its composition included 25% w/w liquid propylene glycol (PG, $C_3H_8O_2$) and 25% w/w potassium acetate (KAC, CH_3COOK), with the remaining 50% consisting of deionized water, which serves as the base solvent.

Figure 16: Runway De-Icing-Icing Products (KFO, KAC, and PG Hybrid)

The anti-icing mode was performed for the three fluids under the ice condition. A consistent volume of 0.7 mL of the de-icing product was applied directly onto the cleaned surface of the concrete sample. This amount of fluid was selected based on recommendation of aerospace standards on ice melting [98]. The controlled application, performed using a spray, ensured uniform coverage of the RDP across the surface. After the application of the RDP, the surface was exposed to freezing drizzle. A specialized nozzle (Nozzle #650017) was used for this purpose, producing droplets with a median volumetric diameter of 115 µm.

The freezing drizzle was applied at a targeted intensity of 8.5 g/dm²·h and a controlled temperature of -5°C, closely replicating real environmental conditions on icy runways [8]. To evaluate the performance

of the fluids at different icing times, icing was conducted for specific durations of 5, 10, 15, and 20 minutes. These intervals were chosen to analyze how friction behavior changes over time in the presence of RDPs under icing conditions.

The de-icing mode was implemented under the removed snow condition using the RDP KFO. In this setup, the accumulated snow was partially removed, and the fluid was uniformly sprayed over the remaining layer. Three sprays were applied, corresponding to approximately 0.3 mL of fluid. After depositing the fluid, we waited 2 minutes before starting the MTA friction test to allow the product to act before testing. This waiting period is similar to the dwell time in winter maintenance operations, where de-icing and anti-icing fluids require time to interact with contaminants before assessing their effectiveness.

Cold Chamber

To achieve the desired icing conditions for this research, we utilized the 4-meter cold chamber at the AMIL. This is one of the five cold chambers available at AMIL, specifically designed for the experimental simulation of freezing drizzle on small to medium-sized samples. The chamber features a double-glazed window that prevents condensation, allowing for clear external observation of the tests being conducted inside.

The cold chamber is capable of simulating medium-sized particles, averaging around 200 μm in diameter. The test section of the chamber measures 2.4 m x 1.5 m x 4.3 m, providing ample space for testing under controlled conditions. The air temperature within the chamber can be precisely regulated, with a range between 10°C and -30°C, which enables researchers to replicate various winter conditions.

The chamber is divided into two distinct sections, as illustrated in Figure 17. The first section is the testing area, equipped with an air exchanger that ensures the delivery of cold air at a consistent and uniform flow throughout the space. This uniform airflow is crucial to maintaining the accuracy and reliability of the test results. The second section is designated for complementary operations, such as the setup of additional devices and equipment. This layout allows for easy manipulation of experimental setups while ensuring that the testing environment remains undisturbed.

The overall design and structure of the chamber were developed to ensure precise control over the conditions, making it an essential tool for simulating freezing drizzle and assessing the effectiveness of anti-icing materials under winter conditions.

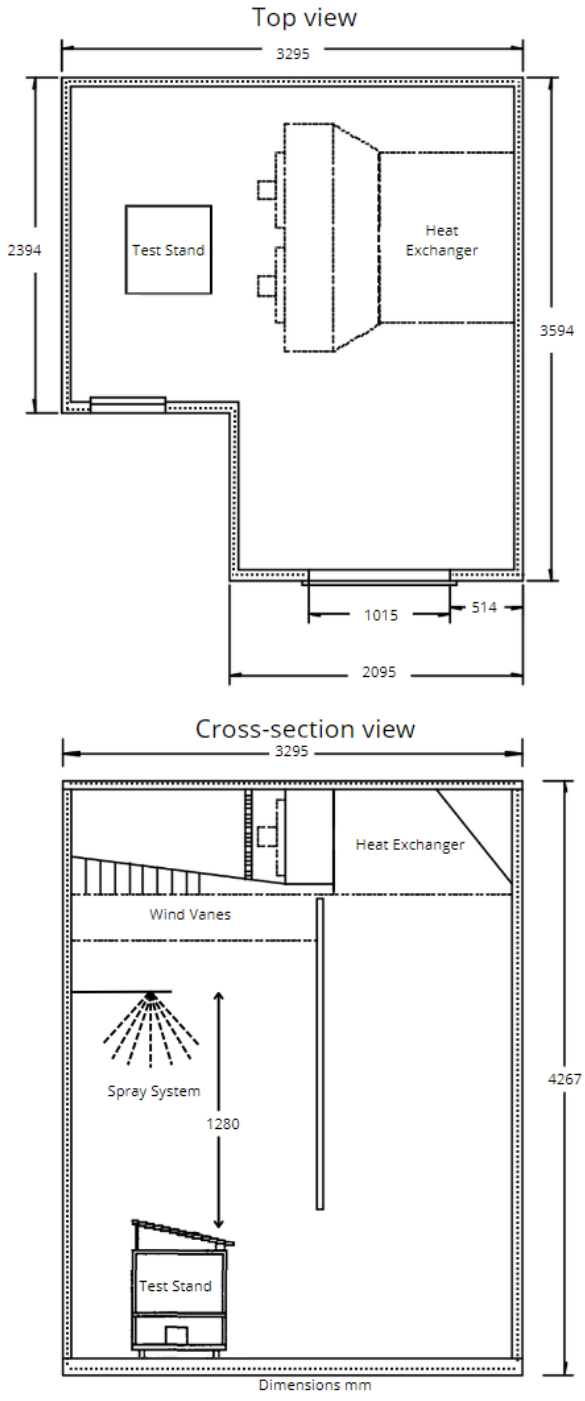

Figure 17: AMIL's 4-meter cold chamber, top (above) and cross-section view (below).

Concrete specimens

The concrete specimens used in the experiment measured 10 cm × 20 cm × 5 cm and were selected for their ability to closely replicate the surface properties of typical Canadian airport runways, particularly in terms of roughness and absorption (as shown in Figure 18).

Figure 18: Concrete samples after icing in the cold room.

Before exposing the samples to icy conditions, they were thoroughly cleaned using deionized water and dried at room temperature. The specimens were then placed in the cold room of the AMIL, where the temperature was carefully maintained at -5°C ± 0.1 °C. Once the samples reached the target temperature, monitored and controlled using a thermocouple, they were subjected to a controlled winter precipitation for a designated time.

Once the precipitation is completed, in order to ensure uniform cooling and stabilize the concrete condition at a temperature of -5 ± 0.5 °C, an interval of at least one hour was allowed between the icing process and the start of the friction test. This waiting period ensured that any latent heat produced during icing had dissipated. Once the preconditioning phase was completed, each iced concrete specimen was tested individually using the MTA to assess its friction properties.

Rubber attachment

We chose to use 100% recycled vulcanized rubber for the rubber component in this research due to its cost-effectiveness, sustainability, and ability to replicate the frictional interactions between aircraft wheels and concrete surfaces. This decision was made carefully, considering both economic factors and the technical requirements of simulating aircraft tire carcasses in our friction measurement setup. The rubber attachment was 3D printed and then glued to the MTA attachments support. Additionally, the same rubber sample was used across all tests to ensure consistency in friction measurements and eliminate variability due to material differences. Given that this was our first time using this specific setup to measure friction under these conditions, opting for recycled rubber provided a balanced solution, allowing us to maintain performance while reducing overall costs [99].

In the aviation industry, natural rubber is commonly used for tire tread carcasses due to safety reasons. Natural rubber tends to have a smoother surface compared to recycled rubber, primarily because it contains fewer additives, impurities, or contaminants. The surface roughness of natural rubber typically falls within the range of 0.1 to 1 μm, whereas recycled rubber can exhibit roughness values ranging from 6 to 55 μm, depending on its processing and composition [100, 101].

The roughness of the rubber surface plays a crucial role in determining the strength of the bond at the interface during contact, which, in turn, affects friction performance. Measuring surface roughness is a crucial step to evaluate how the rubber interacts with concrete surfaces and predicting its wear and performance under operational conditions. Higher roughness, combined with a more irregular surface profile, tends to improve the material's capacity to attract and retain liquids, while also providing insights into the extent of surface damage following frictional contact with concrete [102, 103].

In this study, recycled rubber was used instead of natural rubber, leading to differences in roughness and wear characteristics. These differences were addressed through a mathematical model, which incorporated the measured roughness values of the tested rubber and compared them to typical roughness values reported for aircraft tire treads. This approach allowed for a quantitative assessment of how material variations influence friction behaviour, ensuring that the findings remain applicable to real-world natural rubber tires.

To further examine the surface characteristics of the recycled rubber, we conducted detailed surface roughness measurements using a 3D optical profilometer. This device employs white light interferometry to create detailed topographical maps of a given zone or profile of the rubber's surface. The measurements were performed using a straightforward recipe setup designed specifically for topography analysis. Data analysis was carried out using Profilm3D software, and the surface waviness and roughness heights were evaluated in line with the ISO 4287-1997 guidelines. The tests were conducted using magnification lenses of 20x and 50x, which provided measured areas of 1 x 0.84 mm and 0.4 x 0.34 mm, respectively [104, 105].

3.3 Conclusion

The experimental procedures presented in this chapter display the testing devices, parameters and conditions for the MTA characterization and the friction tests at variable normal force and velocity. It also describes the cold room where the freezing drizzle is generated to simulate winter conditions. This chapter explains the material selection analysis and describes the roughness test with the corresponding standard regarding the rubber attachment.

Chapter 4: Results and Discussion

4.1 Introduction

Building on the previously detailed methodology, this chapter focuses on presenting the corresponding results of the explained procedures. A detailed analysis of obtained data and graphs is provided. All friction results are compared with CRFI regulations to assess their compliance with the standards. The roughness values of the rubber attachment are displayed, along with a line plot profile indicating the flattening and sliding direction angles.

As the main component of the MTA validation, we will develop a mathematical model focused on simulating the coefficient of friction between two sliding surfaces using the friction results presented in this chapter. This model starts with Amontons' first law and incorporates Dowson's combined adhesive and ploughing model. The experimental results from the friction tests at varying normal force and velocity were then used to fit the elaborated theoretical model. Additionally, the model uses the rubber roughness data to calculate the yield stress ratio between the concrete and rubber in our experiment. Ultimately, we obtained a linear model from the experimental friction coefficient results of the normal force testing.

4.2 MTA characterization

The load cell is calibrated by applying a known force, which is then transformed into a corresponding voltage output. This process establishes a calibration in the form of a linear relationship between the applied force and the resulting voltage, ensuring consistent and predictable measurements. However, it is important to note that the slope constants in this relationship can differ from one load cell to the next, indicating variations in their calibration. The calibration results are detailed in Figure 19, providing insight into the performance and accuracy of the load cell used in this study.

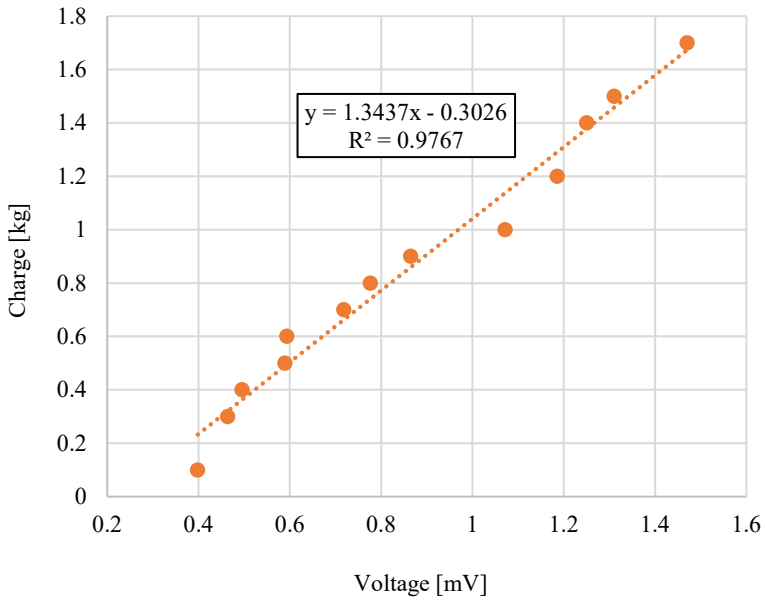

Figure 19: Example of Load cell calibration graph.

The relationship between voltage and force was established through linear regression, as shown in Figure 19. Calibration data points were obtained by gradually increasing the load from 0 kg to 1.8 kg, which was selected based on the expected force range during friction measurements. The resulting graph demonstrates a strong linear trend, with an R^2 value of 0.98. This indicates that 98% of the variance in force measurements is accurately predicted by the voltage output, with the remaining 2% attributed to factors such as sensor noise, slight mechanical inconsistencies, or minor measurement errors.

With an R^2 of 0.98, the load cell calibration can be considered highly reliable, ensuring that future conversions of voltage to force will be precise. Although minor variability remains, the calibration provides confidence in the accuracy of force measurements during experimental procedures.

A comprehensive speed check was conducted to accurately determine the specific speeds corresponding to the frequency values selectable on the MTA. This process was essential in establishing a clear relationship between the frequency settings and the device's actual speed, ensuring that the MTA operates within precise parameters for friction testing. The results of this speed verification are presented in the following Table 4, showcasing the measured speeds for each frequency value.

Table 4 : Frequency equivalent speed – Speed check test.

Frequency (Hz)	Speed [m/sec]	Speed [mm/sec]	Speed Change Rate [(mm/sec)/Hz]
5.00	0.003	2.65	-
6.76	0.004	3.50	0.4830
10.00	0.005	5.06	0.4815
13.96	0.007	7.00	0.4899
20.00	0.010	10.00	0.4967
27.74	0.014	14.00	0.5169
30.00	0.015	15.17	0.5177
55.39	0.028	28.00	0.5051
60.00	0.030	30.33	0.5054
96.92	0.049	49.00	0.5056
100.00	0.051	50.56	0.5065
141.65	0.070	70.00	0.4666
150.00	0.074	73.90	0.4667

These speed measurements are critical for the upcoming friction tests described in this chapter. By understanding how the MTA responds to different frequency inputs, we can ensure that the conditions during the friction experiments are consistent. This insight is foundational to ensuring the validity of the friction tests and contributes significantly to the overall accuracy of the research findings.

3D Profilometry Tests

The profilometry analysis of the rubber attachment was conducted once before the MTA friction tests. The Table 5 displays the surface roughness values generated by the 3D optical profilometer on the rubber pad. Since this instrument is designed to measure small surface areas, six measurements were taken across the rubber sample. The average surface roughness values for the 20x and 50x magnification lenses were 25.2 ± 4 μm and 31.6 ± 11 μm, respectively. These values reflect the variability in the rubber's surface roughness across different areas, highlighting the importance of assessing multiple regions to capture the

full range of surface characteristics. This variability is crucial for understanding how surface texture may influence the friction results.

Table 5: Rubber roughness test results.

Lens	Sample	Rq [µm]	Rq Mean value [µm]	Standard Deviation
20X (1 x 0.84 mm)	1	20.61	25.2	4.0
	2	26.84		
	3	28.13		
50X (0.4 x 0.34 mm)	4	21.92	31.6	11.7
	5	44.62		
	6	28.13		

During the 3D profilometry test, we were able to assess not only the surface roughness values but also obtain detailed line profile graphs from each of the measurements taken. Table 6 presents the images generated by the 3D ProfilmOnline software, offering comprehensive views of the surface texture, roughness, and step-height analysis.

This analysis allowed us to generate line profiles, determine the flattening angle (α), which represents the surface deformation angle under the applied load, and calculate the sliding direction angle (θ_1), which defines the orientation of conical asperities relative to the sliding direction (Figure 20).

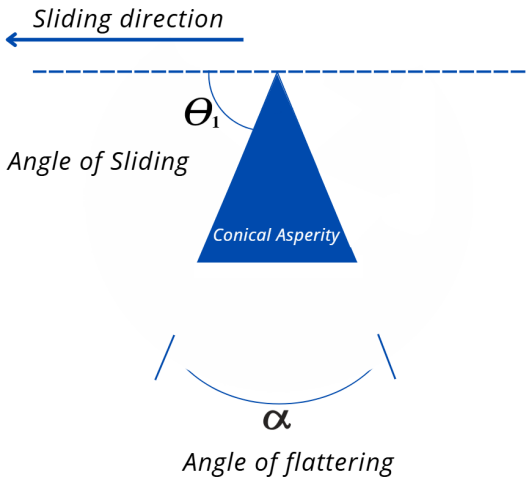

Figure 20: Definition of the Sliding Direction Angle (θ_1) and Flattening Angle (α).

Since surface roughness and deformation influence contact mechanics, θ_1 is included alongside α in Table 6 to capture the directional influence of asperities within the same measurement framework. The combined analysis of these angles provides a more complete characterization of the interaction between roughness features and flattening under loading conditions.

Table 6 : Rubber Attachment 3D Profilometry Results.

Sample	Optical Image of the Sample	Line profile plot	α	θ_1
1	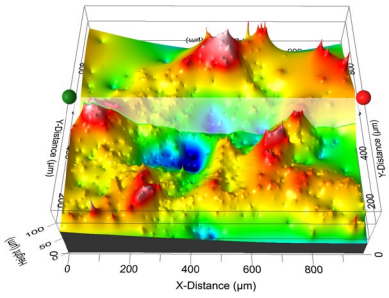	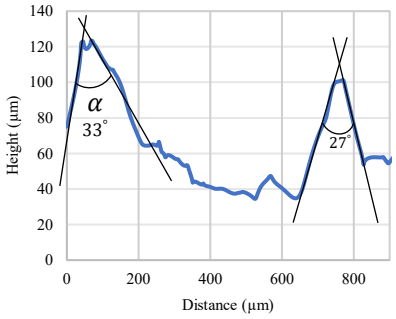	33°	73.5°
			27°	76.5°
2	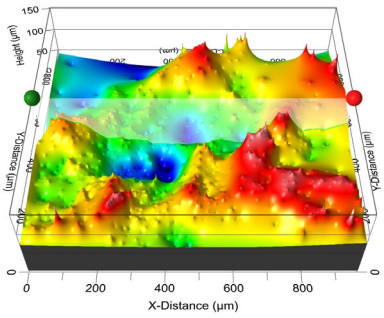	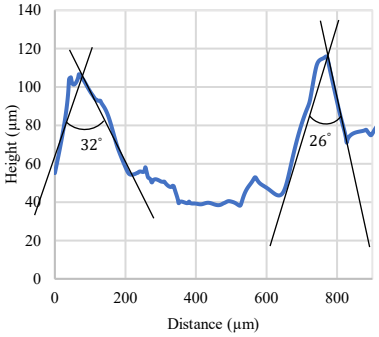	32°	74°
			26°	77°
3	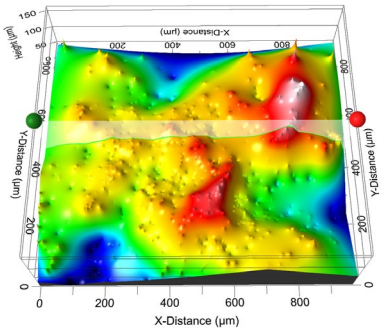	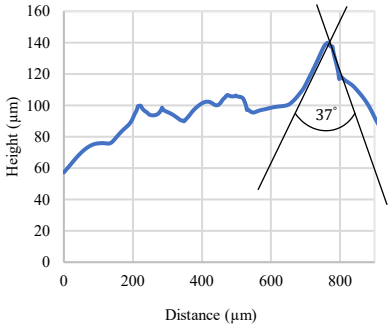	37°	71.5°

4	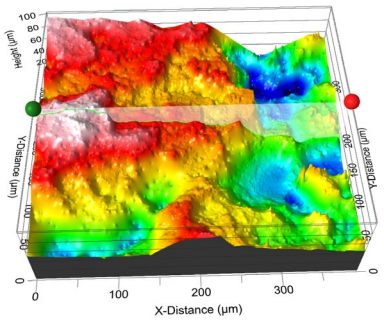	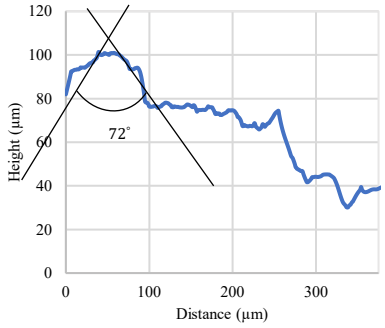	72°	54°
5	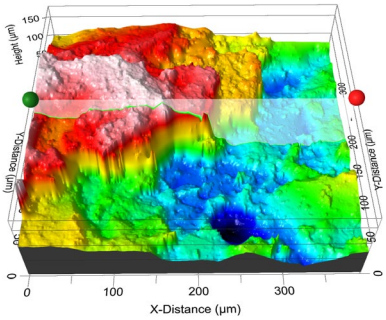	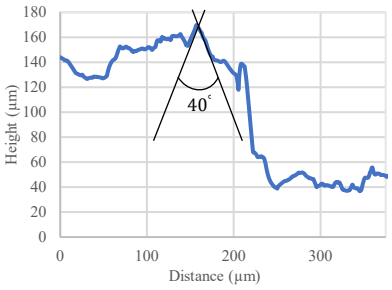	40°	70°
6	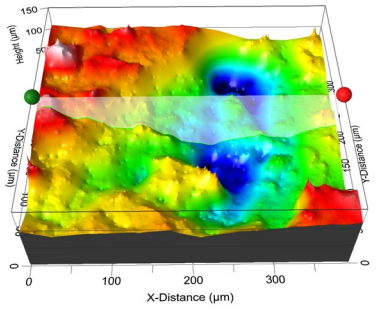	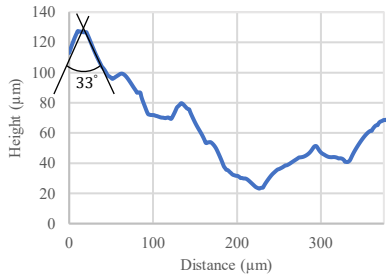	33°	73.5°
	Average		32.6°	71.25°

4.3 MTA Friction Test

To verify the accuracy of the friction values, we used the CRFI, shown in the last column of Table 7. This method helps assess friction levels on Canadian runways. According to the CRFI, dry runways should have a friction value greater than 0.4, while icy conditions should be less than 0.19.

The friction coefficient was determined using the forces recorded as the rubber attachment interacted with the concrete surface during its forward motion. These forces were used to calculate the

friction force, which, combined with the applied normal load, yielded the coefficient. The results for the friction test with the MTA at variable velocity levels are shown in Figure 21.

Table 7 : MTA friction test at variable velocity and constant normal force (226.39N)

Condition	Velocity (m/s)	Friction force (N) $F_{\parallel}$	Friction Coefficient μ	Standard deviation	CRFI Range
Ice	0.004	43.61	0.19	0.051	<0.19
	0.007	42.16	0.19	0.018	
	0.028	40.39	0.18	0.013	
	0.049	35.98	0.16	0.050	
Dry	0.004	207.00	0.91	0.073	>0.4
	0.007	203.23	0.90	0.054	
	0.028	205.02	0.91	0.074	
	0.049	173.21	0.77	0.021	

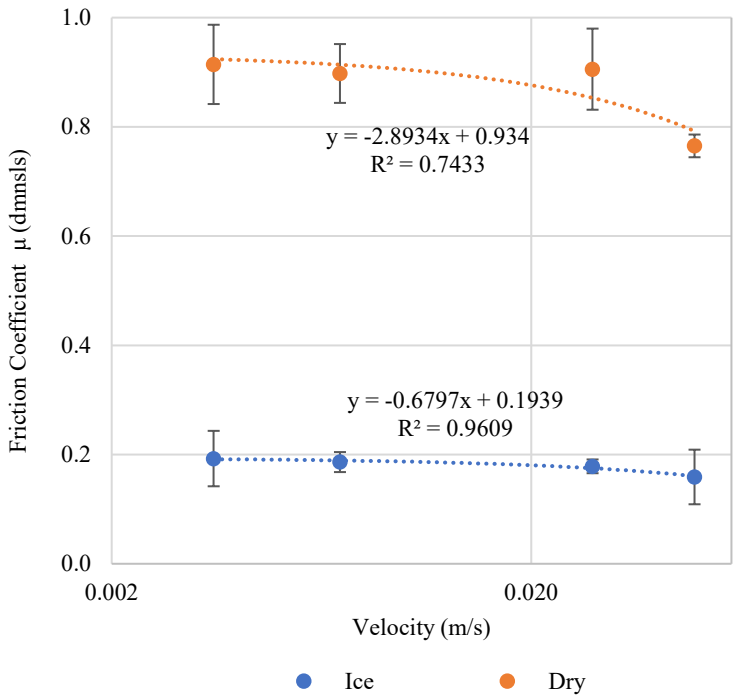

Figure 21: Friction coefficient results at variable velocity with dry and icy concrete.

For icy conditions, friction values remain largely stable, with only a slight decrease at higher velocities. This minor variation does not indicate a strong or consistent relationship between friction and speed, aligning with Amontons' Law, which states that frictional force depends primarily on the applied load and is independent of velocity. To better visualize any subtle variations, a linear regression was applied in the graph, though the observed changes are small. Any deviations from perfect constancy may stem from localized surface interactions, minor melting effects, or experimental factors rather than a fundamental dependence on speed (see Figure 21).

For dry conditions, the linear regression model yields an R^2 value of 0.7433, suggesting a moderate correlation between speed and the friction coefficient. While this may indicate a slight trend of decreasing friction with increasing velocity, the overall variability in the data suggests that velocity alone is not the primary influencing factor. Instead, friction in dry conditions may be affected by surface roughness, micro-scale deformations, or variations in material interactions. The findings reinforce that, despite small fluctuations, friction remains largely independent of velocity, consistent with theoretical expectations.

The results of the variable normal force friction test are presented in Table 8. Each value represents the average of five measurements, with friction measured on each of the five concrete specimens at every pressure level. For the dry, wet with water and ice condition we measured the friction response at different normal load values in order to evaluate the response of the MTA in the whole range of normal forces that the machine can reach (from 62.63 N to 226.39 N), see Figure 22.

Table 8 : MTA friction test at variable normal load with constant velocity (0.007 m/s)

Condition	RWYCC	Pressure (PSI)	Normal Force (N) $F_{\perp}$	Friction Force (N) $F_{\parallel}$	Friction coefficient μ	Standard deviation	CRFI Range	Acceptance range (<10%)
Dry	6	10	62.63	11.15	0.18	0.002	>0.4	No 55%
		20	86.03	24.72	0.29	0.026		No 28%
		30	109.42	38.39	0.35	0.002		No 12%
		40	132.81	55.57	0.42	0.008		Ok
		50	156.20	82.80	0.53	0.013		Ok
		60	179.60	109.39	0.61	0.013		Ok

		70	202.99	130.15	0.64	0.006		Ok
		80	**226.39**	155.14	**0.69**	**0.010**		Ok
Wet with water	3	10	62.63	9.49	0.15	0.006	0.30-0.34	No 49%
		20	86.03	18.07	0.21	0.006		No 30%
		30	109.42	27.05	0.25	0.014		No 18%
		40	132.81	36.05	0.27	0.012		Ok 9.5%
		50	156.20	47.02	0.30	0.017		Ok
		60	179.60	55.80	0.31	0.012		Ok
		70	202.99	65.03	0.32	0.009		Ok
		80	**226.39**	73.97	**0.33**	**0.014**		Ok
Ice	1	10	62.63	7.10	0.11	0.018	<0.19	Ok
		20	86.03	9.34	0.11	0.014		Ok
		40	132.81	15.61	0.12	0.012		Ok
		80	**226.39**	42.16	**0.186**	**0.018**		Ok
Snow	3	80	226.39	38.57	0.17	0.015	0.30-0.34	43%
				44.62	0.20	0.012		34%
				38.48	0.17	0.006		43%
				41.63	0.18	0.008		39%
				39.76	0.18	0.005		41%
				49.07	0.22	0.004		28%
				43.28	0.19	0.004		36%
				43.17	0.19	0.006		36%
				39.74	0.18	0.002		41%
				37.93	0.17	0.004		44%
Removed Snow	3	80	226.39	48.97	0.22	0.007	0.30-0.34	28%
				60.85	0.27	0.005		Ok 10%
				40.73	0.18	0.004		40%
				61.95	0.27	0.005		Ok 9%
				46.26	0.20	0.005		32%

57.83	0.26	0.010	15%
50.35	0.22	0.011	26%
51.38	0.23	0.009	24%
49.78	0.22	0.002	27%
43.66	0.19	0.004	36%

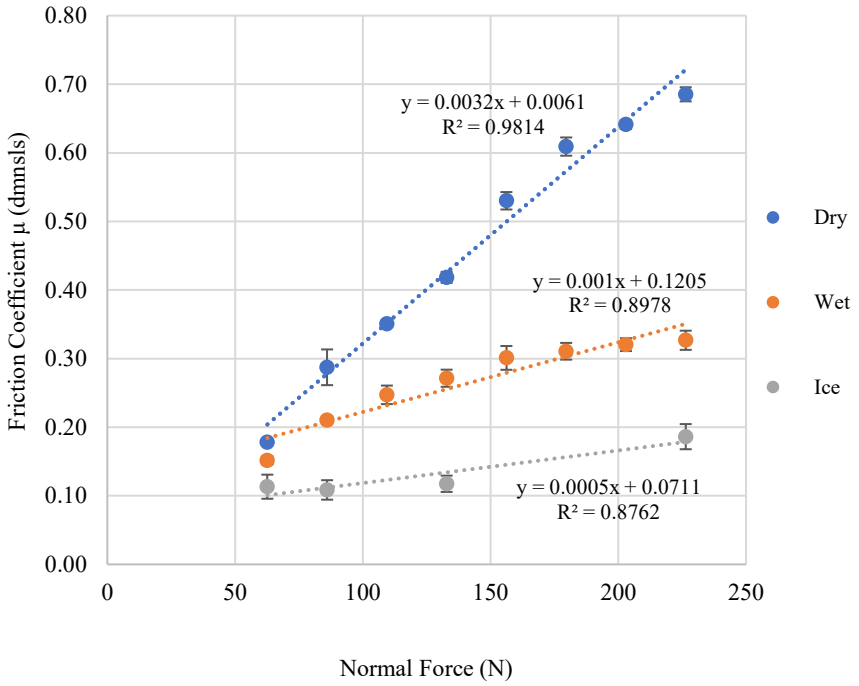

Figure 22: Friction results at variable normal force (F⊥) with dry, wet, and ice conditions.

The results indicate that the friction coefficient increases with higher normal force, which contrasts with the classical assumption that friction remains independent of load. This behavior can be attributed to the viscoelastic properties of rubber, which allow it to deform under pressure, increasing the real contact area with the concrete surface. Unlike rigid materials, rubber conforms to surface asperities under greater loads, leading to enhanced adhesion and plowing effects. This effect is particularly relevant in high-deformation contact scenarios, where deviations from Coulomb's friction model are commonly observed [47]. As a result, the highest friction coefficient was measured on clean concrete, while the lowest was on ice, aligning with the RWYCC classification of poor braking action.

The data point for each condition in the graph follows a constant increment which refers to a consistent performance of the device in terms of friction measurement with high repeatability and low variation between measurements. The variability in μ represented by the standard deviation is minimal, particularly at higher normal forces.

Considering the results of the variable normal load, we decided to perform the test with the rest of the conditions at 226.39 N, which is the highest normal force of MTA. This value offers low variation and more stability, creating a more consistent contact between the two surfaces and avoiding the influence of other surface phenomena at the interface.

Regarding compliance with the CRFI range, the results showed that at higher normal forces, the friction values aligned more closely with the standards, particularly in dry and wet conditions. However, this alignment occurs within the MTA normal force limits (maximum normal force of 226 N). If the normal force were further increased, friction values might exceed the CRFI range due to enhanced rubber deformation, increased real contact area, and stronger adhesion effects, which are not fully accounted for in standardized correlations.

Ice condition response at different normal forces fit well with CRFI values with a friction coefficient lower than 0.19. For snow and removed snow conditions, the results are lower than expected, corresponding to a RWYCC that matches more with ice and slush values (see, Figure 23).

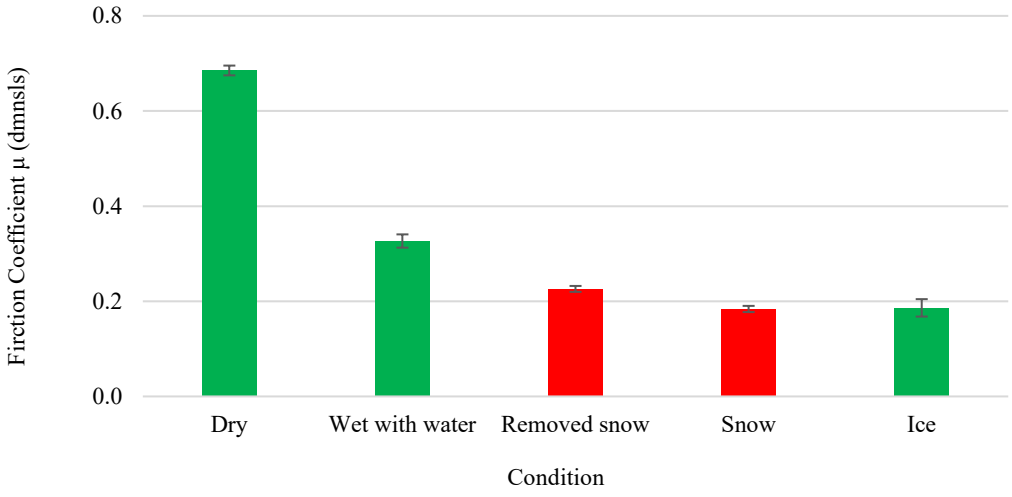

Figure 23: Friction coefficient μ results at 226 N normal force and 0.007 m/s velocity. Green = compliant with GRF standards; Red = non-compliant.

Measuring friction in snow-contaminated concrete and compacted snow can be challenging. The friction behavior in snow depends on its compaction, density, and moisture content. If the snow was looser or wetter than expected, it could have reduced the coefficient of friction, leading to a lower value than anticipated. In snow-ploughed conditions, residual snow particles or ice layers could have formed a lubricating layer with increased viscosity, reducing friction by decreasing direct contact between the rubber and the surface. The higher the viscosity of this layer, the more it behaves like a fluid, further diminishing the ability of the surface to generate traction.

The challenges in measuring friction under snow conditions observed in this study are consistent with the finding from Tan et al. [61]. Their study evaluated the effectiveness of the Dynamic Friction Tester (DFT) in assessing skid resistance under eight winter surface conditions. Their research highlights that even minimal snow coverage significantly reduces friction coefficients and demonstrates that friction coefficients are highly influenced by ambient temperature.

Conventional methods for measuring friction on snow-covered surfaces face several limitations, mainly due to the variability and complexity of such conditions. For example, variations in snow density, grain structure, temperature fluctuations, and moisture content contribute to unpredictable frictional behavior, making it difficult to establish consistent measurements. One significant issue is the variability in friction measurements, which can be attributed to microscopic and nanoscopic surface properties such as ice crystal morphology, surface roughness of both ice and rubber, and the presence of thin liquid water films at the interface. These factors are difficult to control and can lead to inconsistencies in results, even under controlled laboratory conditions [106]. This variability becomes more pronounced with the presence of snow, which can greatly decrease friction levels, as evidenced by experiments showing a marked decrease in friction coefficients with minimal snow contamination.

Widely used friction measurement tools, such as the British Pendulum Tester, may not fully capture the frictional behavior of snow-covered surfaces due to spatial variability and their inability to simulate the rolling motion of tires, which is fundamental in practical applications [107]. The issue is compounded by the fact that these devices usually deliver only single-point measurements, failing to represent the ongoing

frictional interactions across a broader area. Moreover, the presence of snow modifies the surface texture, affecting both microtexture and macrotexture, which are crucial for accurate friction assessment.

The frictional behavior on snow is influenced by various factors such as temperature, snow compaction, and the presence of an ice interlayer and liquid water, which are not always adequately accounted for in traditional measurement approaches [108]. These limitations highlight the need for more advanced and adaptable methods that can provide real-time, comprehensive assessments of friction on snow-contaminated surfaces, considering the complex and variable nature of these conditions.

4.4 Friction Test with Runway De-icing Products

In this part of the study, we evaluated the performance of three liquid RDPs under two different conditions: ice and removed snow. For the ice condition, we tested the anti-icing effectiveness of all three fluids. For the removed snow, we focused only on testing KFO to confirm its good performance in such conditions, as reported in previous studies [8]. This approach allowed us to verify the reliability of the MTA in accordance with the findings of other similar investigations.

For the anti-icing tests, friction was first measured under dry conditions, and the same concrete samples were then used to measure friction in the wet condition (Figure 24). This approach allowed for a direct comparison between dry and wet surfaces without introducing variability from different samples.

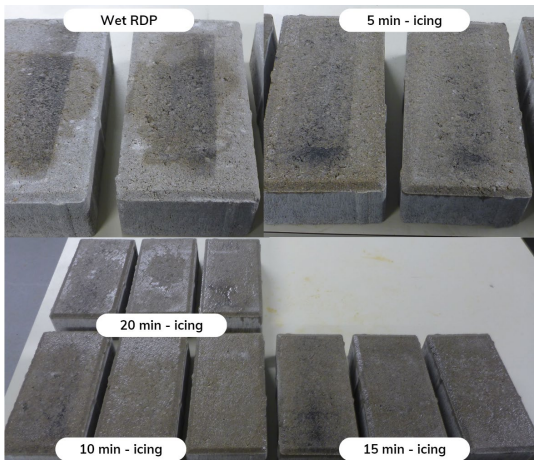

Figure 24: Anti-icing mode test. Concrete samples after each icing time interval (velocity of 0.007 m/s and a normal force of 226 N)

For the ice condition, we tested the anti-icing effectiveness of all three fluids (KFO, KAC, PG Hybrid), taking five measurements per time interval (see, Figure 24). New concrete samples were used at each time

interval. This was done to prevent interference between tests, as some fluid could be removed during measurements, potentially affecting subsequent results. Using fresh samples ensured that each time interval was evaluated independently, maintaining the accuracy of the friction measurements.

On the other hand, for the de-icing test, the snow removal was simulated and then the product (KFO) was applied. After spraying the fluid, we waited two minutes before proceeding with the test (see Figure 25).

Figure 25: De-icing test with removed snow condition and KFO

The main results of the friction coefficient measurements in the presence of liquid RDP's are presented in the Table 9. It shows the average value from the five measurements for each icing time, including the friction force, coefficient of friction, and the corresponding standard deviation.

Table 9: Friction test results for RDPs in anti-icing and de-icing modes, conducted at a normal force of 226 N, a velocity of 0.007 m/s, and a temperature of -5°C.

RDP	Mode	Precipitation	Icing time (Min)	RWYCC	Friction force (N) $F_{\parallel}$	Friction coefficient μ	Standard deviation
-	-	Dry	0	6	234.75	1.04	0.03
KFO	Anti-icing	Ice	Wet with RDP	3	181.91	0.80	0.05
			5	1- wet	232.28	1.03	0.05
			10	1- wet	109.15	0.48	0.02
			15	1 - ice	26.94	0.12*	0.01
			20	1 - ice	19.72	0.09*	0.04
	De-icing	Removed Snow	-	3	165.66	0.73	0.06
				Compacted snow (> -15)	146.08	0.65	0.06
					156.37	0.69	0.12
					158.08	0.70	0.07

					132.85	0.59	0.08
KAC	Anti-icing	Ice	Wet with RDP	3	219.48	0.97	0.04
			5	1- wet	143.26	0.63	0.06
			10	1- wet	177.38	0.78	0.03
			15	1 - ice	33.48	0.15*	0.00
			20	1 - ice	31.21	0.14*	0.00
PG (Hybrid)	Anti-icing	Ice	Wet with RDP	3	208.02	0.92	0.10
			5	1- wet	132.61	0.59	0.08
			10	1- wet	132.36	0.58	0.06
			15	1 - ice	60.99	0.27	0.01
			20	1 - ice	87.54	0.39	0.02

*Friction coefficient values below the ice reference value (0.18)

At the beginning of the icing time, when no precipitation was present, the friction coefficient was similar to the reference value for dry concrete (see Figure 26). However, it slightly decreased, indicating that the de-icing products acted as a lubricant on the surface (see Table 9). After 5 minutes of exposure to freezing drizzle, KAC and PG Hybrid exhibited the typical behavior, with friction decreasing due to the accumulation of winter contaminants on the surface. However, in the case of KFO, the friction increased from 0.8 to 1. This could be due to the surface becoming rougher as the ice began to form, temporarily increasing friction, as you can see in figure 27.

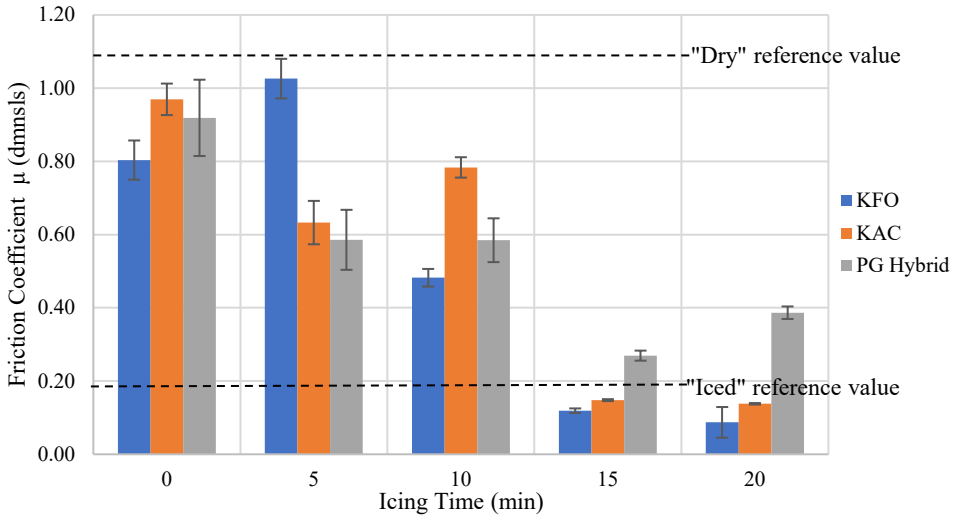

Figure 26: Anti-icing test friction results over time intervals (0, 5, 10, 15 and 20 minutes)

Figure 27: Concrete specimens with surface texture generated by the icing precipitation

At the 10-minute mark for KFO, there is a sharp decline in the friction coefficient, which continues until the end of the test at 20 minutes. This drop occurs as the surface becomes covered by an ice layer, creating a quantification of ‘’smoothness’’. A similar trend is observed with PG Hybrid, though its changes are less drastic. The friction remains relatively stable between 5 to 10 minutes and 15 to 20 minutes.

Interestingly, at 20 minutes, friction slightly increases, which could be due to a specific texture created by ice on the concrete surface. For KAC, friction rises to 0.78 at 10 minutes, likely for the same reason as with PG Hybrid ice formation leading to temporary surface roughness. However, this effect was observed for all tested fluids, suggesting that the interaction between the fluids and the ice led to localized melting and refreezing, resulting in a non-uniform surface texture. This temporary roughness could explain the fluctuations in friction, as opposed to a completely smooth ice layer that would produce consistently lower values.

All fluids demonstrated an ability to enhance concrete friction conditions during the first 10 minutes as their friction levels remained above the iced reference threshold, representing a nearly 83% reduction from the reference. PG Hybrid showed a more stable and efficient anti-icing performance, consistently keeping higher friction values across nearly all-time intervals. Despite using a smaller amount of fluid in this test, this was intentional, as our primary focus was to evaluate the MTA's capability in estimating the laboratory efficiency of RDPs through friction measurements on concrete.

For the de-icing test, we compared the results with the untreated removed snow condition to evaluate how the fluid improved surface conditions using the same type of samples. This behavior is illustrated in Figure 28. Across all samples, the presence of de-icing fluid increased the surface friction coefficient. Notably, KFO demonstrated its effectiveness in both anti-icing and de-icing modes, aligning with the findings of Brassard et al., who described KFO as one of the most effective products for the removed snow condition [8].

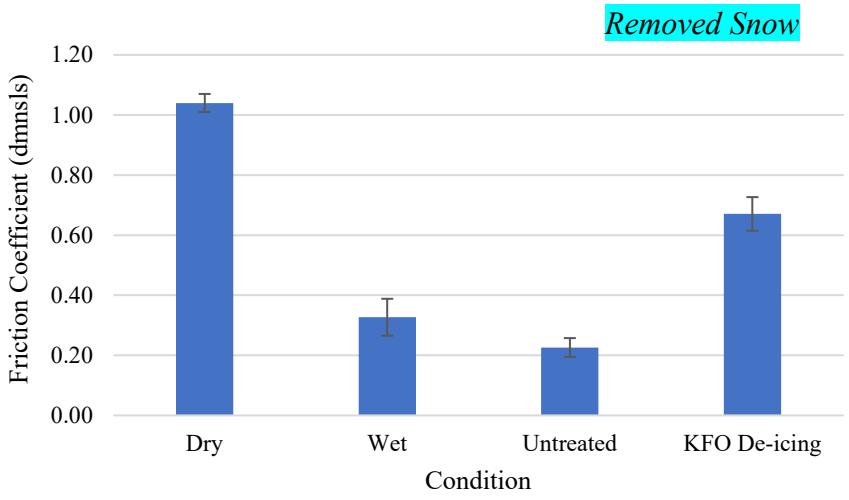

Figure 28: Friction results for removed snow condition (untreated and treated with KFO) compared to wet and dry concrete friction values. At 226 N normal force and 0.007 m/s velocity.

4.5 Mathematical Model

To simulate the MTA's behavior, we developed a mathematical model to estimate the friction coefficient between sliding surfaces. This model is based on experimental friction data obtained in this study and integrates theoretical description of friction principles, starting with Amontons' laws, which were later expanded by subsequent researchers. The model's accuracy will be evaluated using data collected from the MTA.

The study of friction traces back to Leonardo da Vinci's initial observations, later formalized as Amontons' laws, which establish that the frictional force is directly proportional to the applied load and is

unaffected by sliding speed [47, 109, 110]. Amontons' first law is expressed as the relation between the friction force $F_{\parallel}$ and the applied normal force $F_{\perp}$, resulting in the friction coefficient:

$$\mu = \frac{F_{\parallel}}{F_{\perp}} \quad (2)$$

Dowson [111], emphasizes the principal models or approaches developed throughout the long history of friction research. The geometrical or mechanistic model suggests that friction originates from the interaction between surface asperities and the forces needed for these asperities to slip over each other.

The molecular or adhesive model, on the other hand, attributes friction to surface forces and molecular adhesion, with lubricants reducing friction.

Additionally, the deformation or ploughing model attributes friction to the force required to move hard asperities across or into another surface. Here, ploughing frictional force $F_{\parallel}$ is given by:

$$F_{\parallel} = A_0 H' \quad (3)$$

A_0 is the total area of the indenting asperities perpendicular to the direction of sliding and H' represents the rubber yield stress. Similarly, the normal load $F_{\perp}$ is:

$$F_{\perp} = A_{real} H \quad (4)$$

A_{real} represents the actual contact area, and H is the yield stress of the harder material, concrete in this case. This setup allows the model to differentiate friction responses based on surface roughness and hardness.

For conical asperities oriented at an angle θ_1 relative to the direction of sliding (Figure 20), the estimated friction coefficient is:

$$\mu = \frac{A_0}{A_{real}} = \frac{2}{\pi} tan(\theta_1) \quad (5)$$

Recognizing that friction is influenced not only by surface interactions at the molecular level but also by subsurface deformation, we adopted Dowson's combined adhesive and ploughing model. In this context, subsurface deformation extends to the depth where material stress distribution significantly affects

the real area of contact and frictional response, which depends on factors such as load, material hardness, and asperity geometry [111]. This model captures both surface and deeper level deformations, defining the frictional force as:

$$F_{\parallel} = F_{ploug} + F_{sh} \quad (6)$$

The ploughing term is given by equation (3), and the F_{sh} represents the shearing term, expressed as $F_{sh} = A_{real}\, s$, with s representing the tangential stress required to shear the junction. This leads to:

$$\mu = \frac{F_{\parallel}}{F_{\perp}} = \frac{F_{ploug} + F_{sh}}{F_{\perp}} = \left(\frac{A_0}{A_{real}}\right)\left(\frac{H'}{H}\right) + \frac{s}{H} \quad (7)$$

To derive a simplified expression for the friction coefficient, we assume $H = H'$. This assumption allows for a more straightforward initial formulation while maintaining the essential physical behavior of the system. However, both terms are later reintroduced in the model to account for their distinct contributions to the overall frictional response.

$$\mu = \frac{A_0}{A_{real}} + \frac{s}{H} \quad (8)$$

Experimental fitting of measurements to predict the friction coefficient

We measure friction at four different normal force levels (62.63, 86.03, 132.81, and 226.39 N) with dry and ice conditions to fit the experimental data with the theoretical equations. These two conditions were selected due to the availability of more comparative data, allowing for a focused analysis and simplifying the comparison with theoretical models. In this way we plotted the $F_{\perp}\ vs.\ F_{\parallel}$ and $F_{\perp}$ vs. μ data in Figures 29 and 30, and derived the corresponding line equations.

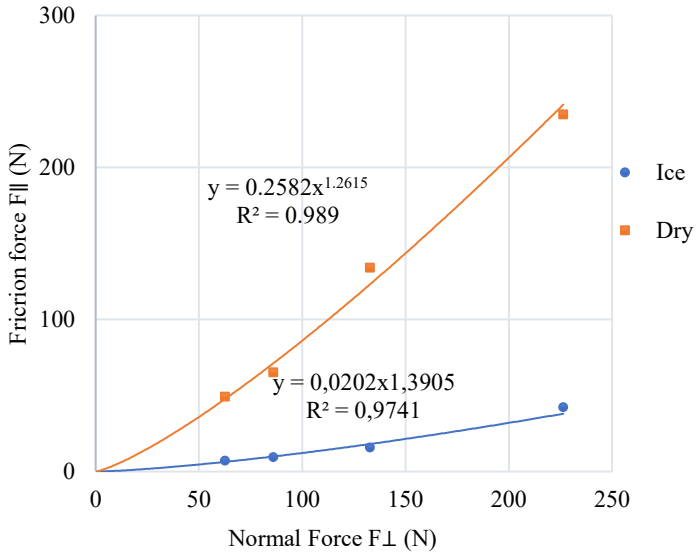

Figure 29: MTA Friction force vs normal force for ice and dry conditions (mathematical model)

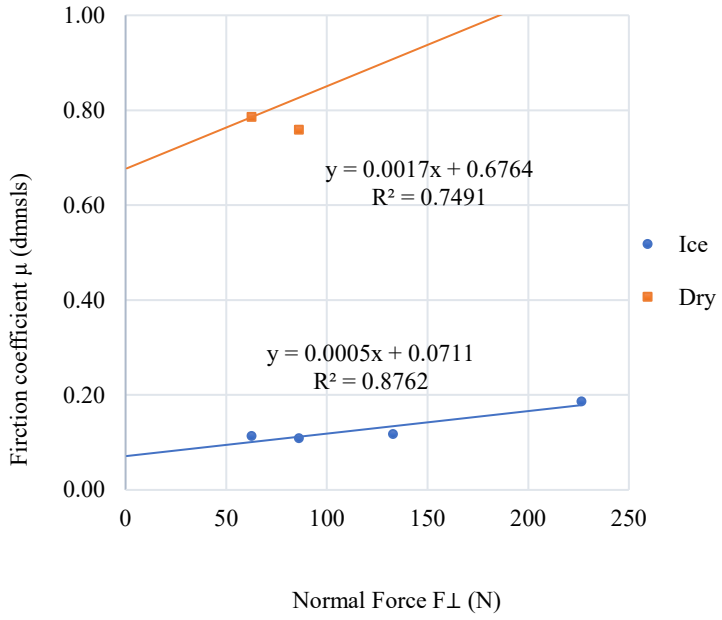

Figure 30: MTA Friction coefficient vs normal force for ice and dry conditions (mathematical model)

The regression models for friction force vs normal force exhibit high R^2 values for both conditions ($R^2 = 0.989$ for dry and $R^2 = 0.9741$ for ice), confirming a strong correlation, though friction on dry surfaces is slightly more predictable. In contrast, the friction coefficient shows greater variability, with a

lower $R^2 = 0.7491$ for dry conditions compared to $R^2 = 0.8762$ for ice, suggesting that friction in ice conditions follows a more consistent trend as normal force increases. This difference may be attributed to greater surface interactions, contact area changes, or material deformation effects in dry conditions, making friction less linear compared to the more uniform behavior observed on ice.

Accordingly, the best exponential and linear fits are written below, following the structure of equation (2):

- Dry conditions:

$$F_{\parallel} = 0.258\, F_{\perp}^{1.261} \qquad R^2 = 0.989 \tag{9}$$

$$\mu = 0.0017\, F_{\perp} + 0.676 \qquad R^2 = 0.7491 \tag{10}$$

- Ice conditions

$$F_{\parallel} = 0.0202\, F_{\perp}^{1.3905} \qquad R^2 = 0.9741 \tag{11}$$

$$\mu = 0.0005\, F_{\perp} + 0.0711 \qquad R^2 = 0.8762 \tag{12}$$

To align the line equations with the adhesive and ploughing theory, we consider the following factors dependence: $F_{\parallel} \propto \mu^* F_{\perp}^{\,a}$, defining equation (8) as:

$$\mu = \mu^* F_{\perp}^{(a-1)} \left(\frac{A_{real}}{A_0}\right) + \frac{2}{\pi} tan(\theta_1) \tag{13}$$

In this way using the experimental values from equation (9) we obtain:

$$\mu = 0.258\, F_{\perp}^{0.261} \left(\frac{A_{real}}{A_0}\right) + 0.676 \tag{14}$$

And the friction coefficient for the dry condition results in:

$$\frac{A_{real}}{A_0} = 6.6\text{x}10^{-3}\text{F}_{\perp}{}^{0.739} \quad (15)$$

In the case of icy conditions, we derived:

$$\mu = 0.0202\ \text{F}_{\perp}{}^{0.3905}\left(\frac{A_{real}}{A_0}\right) + 0.0711 \quad (16)$$

$$\frac{A_{real}}{A_0} = 24.8\text{x}10^{-3}\text{F}_{\perp}{}^{0.609} \quad (17)$$

The MTA over estimates the friction coefficients for dry conditions, indicating that adhesive and ploughing forces are active as the surface asperities engage deeply. In icy conditions, friction coefficients are stable and lower, suggesting limited asperity engagement and less ploughing force.

Using a surface geometry conic modeling to estimate friction coefficient

Following the main structure of the model, we now move to the contact between the two surfaces (rubber and concrete), zooming in on the tiny, cone-shaped rough spots, or asperities, that come into play when they slide against each other. Figure 31 shows this setup. Imagine these asperities as small cones pressing into the other surface, influencing how friction develops through their shape and how they deform under load.

To understand how many of these tiny cones are involved, we can calculate the number in contact with each other. It's a basic estimate that considers the contact area and the size of each asperity:

$$n^{\circ}cone \simeq \frac{L\,W}{4\,r^2} \simeq \frac{A}{4\,r^2} \quad (18)$$

Whose L and W define the dimensions of the overall contact area, and r is the radius of each asperity, see Figure 31.

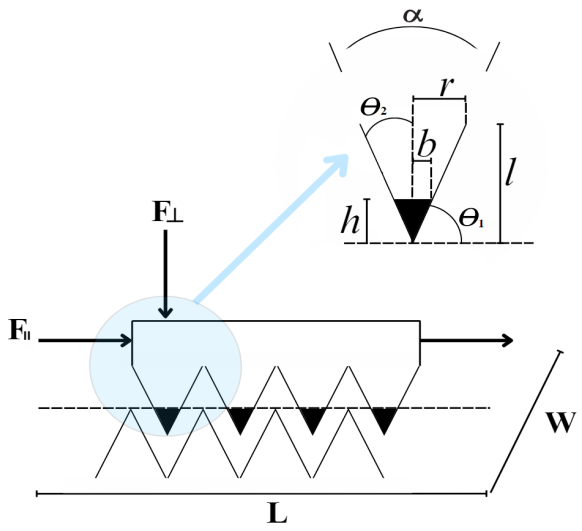

Figure 31: Roughness conic model.

The next step is to determine the real contact area, which represents the actual surface area in contact with the opposing material. Deformation plays a key role here, as asperities flatten under pressure. In this calculation, we assume that the concrete surface is fully rigid and does not undergo significant deformation, while the rubber material deforms. We calculate this area as follows, here b is the deformed radius of the sliding material, in our case rubber:

$$A_{real} \simeq n°cone\ \pi\ b^2 \simeq \frac{A\ \pi\ b^2}{4\ r^2} \qquad (19)$$

To simplify, we approximate the active surface A_0, focusing on half of each cone's projection in the sliding direction. This reasonable approximation gives us a working estimate without diving into each asperity's exact shape, where the term h indicates the height of the flattened asperity:

$$A_0 \simeq \frac{A\ \pi\ b\ h}{4\ r^2\ 2} \qquad (20)$$

In this way to relate the real contact area to the active surface are, we obtained this ratio:

$$\frac{A_{real}}{A_0} \simeq \frac{2\,b}{h} = 2tan(\theta_2) \quad (21)$$

θ_2 represents the angle that defines how much the asperity has deformed. In Figure 31, this relation allowed us to estimate θ_1, as:

$$\theta_1 \simeq tan^{-1}\left(\frac{2A_0}{A_{real}}\right) \quad (22)$$

and the angle α, which indicates the deformation of the surface with the load (flattering):

$$\alpha \simeq \pi - 2\theta_1 \quad (23)$$

Using the Bowden theory of friction to explain the friction coefficient

Now that we've covered how the rubber and concrete asperities interact at the surface, we dive deeper into what happens as we start increasing the load on these asperities. As more pressure is applied, these tiny cones don't just press against each other; they change shape. This brings us to elastic and plastic deformation, two very different ways materials respond to force.

Bowden et al. [112], studied the behavior of asperities that are conical or pyramidal using different experimental set-up and materials. They found that under a heavy load, the real contact area (where the surfaces truly touch) does not just stay the same, it grows. In situations where the asperities yield to the load and plastic flow begins (meaning the deformation is permanent), the real contact area grows according to this relation:

$$A_{real} \simeq k' \, \mathrm{F}_{\perp}{}^{0.8} \quad (24)$$

In other words, this proposal states that the contact area increases at the rate of $\mathrm{F}_{\perp}{}^{0.8}$ with increasing load. The k term is a constant that depends on the material properties and the specific conditions

of the indentation process. It effectively scales the relationship between the load and the indentation geometry. Conversely, the A_{real}, if the load is enough to deform the asperities but not permanently change them (an elastic deformation), we see a slower rate of area increase $F_{\perp}{}^{0.66}$:

$$A_{real} \simeq k'' \, F_{\perp}{}^{0.66} \qquad (25)$$

In this case, k'' adjusts the relationship, but since the material is deforming elastically, it will snap back to its original shape once the load is removed. Rubber exhibits visco-plastic behavior, and in our case, according to Equation (15), the rubber-on-concrete interaction falls between these two extremes, with an exponent of approximately 0.74. This indicates that the rubber is neither purely elastic nor purely plastic, which aligns with the fact that rubber degrades and loses particles over time, particularly on rough surfaces like concrete. Consequently, the rubber experiences gradual wear on the road.

$$\text{Elastic} \rightarrow \quad 0.66 < 0.74 < 0.8 \quad \leftarrow \textit{Plastic} \qquad (26)$$

The behavior of the rubber sliding on concrete does not fit perfectly into purely elastic or purely plastic deformation models. The material properties of rubber, combined with the texture and hardness of concrete, likely result in a deformation response that is not purely one type (visco-plastic).

Using the effect of yield strength to estimate the friction coefficient – Theoretical Model

Now, we add an additional layer by considering the yield strength ratio between rubber and concrete. Initially, in Equation (8), we assumed the yield strength $\frac{H'}{H} \simeq 1$; however, this assumption does not hold true in practice for different materials in contact. The yield strength of concrete is significantly higher than the one of rubber, ranging from 21 MPa to 28 MPa [113], while the tensile strength of rubber varies from 4.5 MPa for old tires to 11.5 MPa for new tires [114]. Therefore, we define a yield strength ratio, $\beta = \left(\frac{H'}{H}\right)$, which, in our case, lies between 0.16 and 0.55.

To determine our value of β, we used the data from equation (14), where $b_0 = 0.676$, along with 3D profilometry results (Table 6), which show an average flattering angle of $\bar{\alpha} = 32.6°$. These values result

in a yield-strength ratio of $\beta \simeq 0.4$, which falls within our expected range for rubber-on-concrete interactions. For rubber sliding on dry concrete, considering the effect of yield stress, this result is acceptable, as it meets the criterion $0.16 < \beta \simeq 0.4 < 0.55$, based on yield stress values.

As we can see, the values of β can vary by a factor of three depending on the possible values of the yield strength of the rubber and concrete. For this reason, for the study, we selected the β value that minimize the prediction error of the theoretical model. For dry conditions, a yield stress ratio of 0.16 was used. In icy conditions, a value of 0.045 was chosen, calculated by considering the H of rubber on ice and referencing standard material values [47]. This approach ensured that the theoretical model provided the most accurate predictions for each specific condition.

Bringing β into the friction coefficient equation refines it to reflect the real yield stress differences:

$$\mu = 2\mu^* tan\left(\frac{\bar{\alpha}}{2}\right) F_{\perp}^{(a-1)} + \frac{\beta}{2} cotan\left(\frac{\bar{\alpha}}{2}\right) \quad (27)$$

To fit the previous theoretical model equation (27) to the linear model structure $\mu = mF_{\perp} + b_0$, we enforce the following conditions to ensure it conforms to a linear model:

$$\mu = \left[2\mu^* tan\left(\frac{\bar{\alpha}}{2}\right) F_{\perp}^{(a-2)}\right] F_{\perp} + \left[\frac{\beta}{2} cotan\left(\frac{\bar{\alpha}}{2}\right)\right]$$

where

$$m = 2\mu^* tan\left(\frac{\bar{\alpha}}{2}\right) F_{\perp}^{(a-2)} \qquad and \qquad b_0 = \frac{\beta}{2} cotan\left(\frac{\bar{\alpha}}{2}\right)$$

Fitting a linear model of friction using the Bowden's theory

To further validate the mathematical model, we incorporated a linear fitting approach to describe the relationship between the friction force ($F_{\parallel}$) and normal force ($F_{\perp}$). By taking the derivative of the friction coefficient μ as a function of $F_{\perp}$ (Eq. 28-31), we obtained an expression for the rate of change of μ concerning $F_{\perp}$.

$$\mu = \frac{F_{\parallel}}{F_{\perp}} = \mu^{*} {F_{\perp}}^{(a-1)} \quad (28)$$

$$\frac{d\mu}{dF_{\perp}} = \mu^{*}(a-1){F_{\perp}}^{a-2} \quad (29)$$

$$\frac{d\mu}{dF_{\perp}} = \mu^{*}{F_{\perp}}^{a-1}\frac{(a-1)}{F_{\perp}} \quad (30)$$

$$\frac{d\mu}{dF_{\perp}} = \mu\frac{(a-1)}{F_{\perp}} \quad (31)$$

Now, considering the structure of the line equations (10) and (12)

$$\mu = mF_{\perp} + b_0 \quad (32)$$

We get the equation to compute the slope m_i for each data sample i:

$$m_i = \mu_i \frac{(a-1)}{F_{\perp_i}} \quad (33)$$

Each calculated m_i represents how the friction force changes relative to the normal force for each sample, capturing the unique response in that test. Similarly, to obtain the expression for b_{0_i} we used equation (32) and derived the following equation. Each b_{0_i} provides the baseline friction coefficient when extrapolated to zero applied load, allowing us to isolate the inherent friction characteristics of the surface under each test condition:

$$b_{0_i} = (2-a)\mu_i \quad (34)$$

In this way, the linear model is defined as:

$$\mu(F_{\perp}) = \frac{\mu_i\,(a-1)}{F_{\perp_i}}F_{\perp} + (2-a)\mu_i \quad (35)$$

with the average of the set values:

$$\bar{m} = \frac{\Sigma m_i}{i} \qquad and \qquad \overline{b_0} = \frac{\Sigma b_{0_i}}{i} \tag{36}$$

Together, the average slope $\bar{m}$ and intercept $\overline{b_0}$ offer a way to generalize the friction behavior seen across multiple tests, giving a clearer picture of how the material typically performs under standard loads. Including a linear fit strengthens the model by aligning it with current data, which in turn allows for reliable predictions about friction even in conditions not specifically tested.

Predictions of friction coefficient using Bowden (theoretical) and linear models

Finally, using the theoretical and linear models, we calculated the friction coefficient and compare the results with the experimental data. All calculations were performed using the MTA results obtained during the variable normal force tests, see Table 10.

Table 10 : Friction coefficient predictions: models vs. experimental results from the normal force test

Condition	Pressure (PSI)	Normal Force (N) $F_\perp$	μ experimental	Standard deviation	Theoretical Model μ	Theoretical Model % error	Linear Model μ	Linear Model % error
Ice	10	62.63	0.113	0.018	0.097	14.7	0.109	3.5
	20	86.03	0.109	0.014	0.108	0.2	0.120	10.7
	40	132.81	0.118	0.012	0.132	12.1	0.142	20.9
	80	226.39	0.186	0.018	0.179	4.1	0.186	0.3
		Average				***7.8***		***8.8***
Dry	10	62.63	0.18	0.002	0.19	8.65	0.19	5.54
	20	86.03	0.29	0.026	0.27	6.63	0.27	7.48
	30	109.42	0.35	0.002	0.34	2.21	0.34	2.02
	40	132.81	0.42	0.008	0.42	0.10	0.42	0.80
	50	156.20	0.53	0.013	0.49	7.02	0.50	5.73
	60	179.60	0.61	0.013	0.57	6.79	0.58	5.16
	70	202.99	0.64	0.006	0.64	0.22	0.66	2.25
	80	226.39	0.69	0.010	0.72	4.69	0.73	7.05
		Average				***4.5***		***4.5***
Wet with water	10	62.63	0.15	0.006	0.18	20.98	0.18	21.59
	20	86.03	0.21	0.006	0.21	1.60	0.21	0.49

	30	109.42	0.25	0.014	0.23	6.89	0.24	3.72
	40	132.81	0.27	0.012	0.25	6.59	0.26	2.41
	50	156.20	0.30	0.017	0.28	8.01	0.29	3.09
	60	179.60	0.31	0.012	0.30	3.34	0.32	2.53
	70	202.99	0.32	0.009	0.32	1.04	0.35	7.82
	80	226.39	0.33	0.014	0.35	6.24	0.37	13.95
		Average				***6.8***		***7.0***

The theoretical and linear models presented friction results close to the experimental findings. In the case of the ice condition, the percentage of error for the theoretical model is lower with 7.8% compared to the linear model with 8.8%. For dry conditions, both models obtained the same error of 4.5%, the lowest of the three conditions. Finally, the wet condition with water presented comparable results with an error of the theoretical model of 6.8% and the linear one of 7%. Both models showed reasonable accuracy, with the theoretical model slightly outperforming the linear model.

The theoretical model friction incorporating different friction effects is a more robust model in comparison with the linear model to predict values with different surfaces and load conditions.

The results indicate the predictive capacity of both models and help to validate the MTA as a reliable friction measurement tool, thanks to the alignment with friction theory, reflected in the low error when comparing the experimental data with the predictions of the theoretical model.

Figure 32 shows for each condition the predicted values of the coefficient of friction for the entire range of normal force of the MTA. In the case of the ice condition, we added the predictions of the theoretical model for the entire normal force values to evaluate the predictive response of the model.

Under all conditions there is a specific tendency for the coefficient of friction to increase as the normal force is increased, and both models followed this pattern. The theoretical model predictions of ice conditions were able to show the expected behaviour of friction, unlike the linear model which, based on experimental data, is limited in predicting all values such as this case.

The theoretical model offers greater overall accuracy, especially under conditions where the material's surface characteristics and stress distribution are key factors (e.g., high pressures). While the

linear model, is simpler, it provides reliable results under lower and moderate pressures, making it a practical option for scenarios that do not require a complex predictive tool.

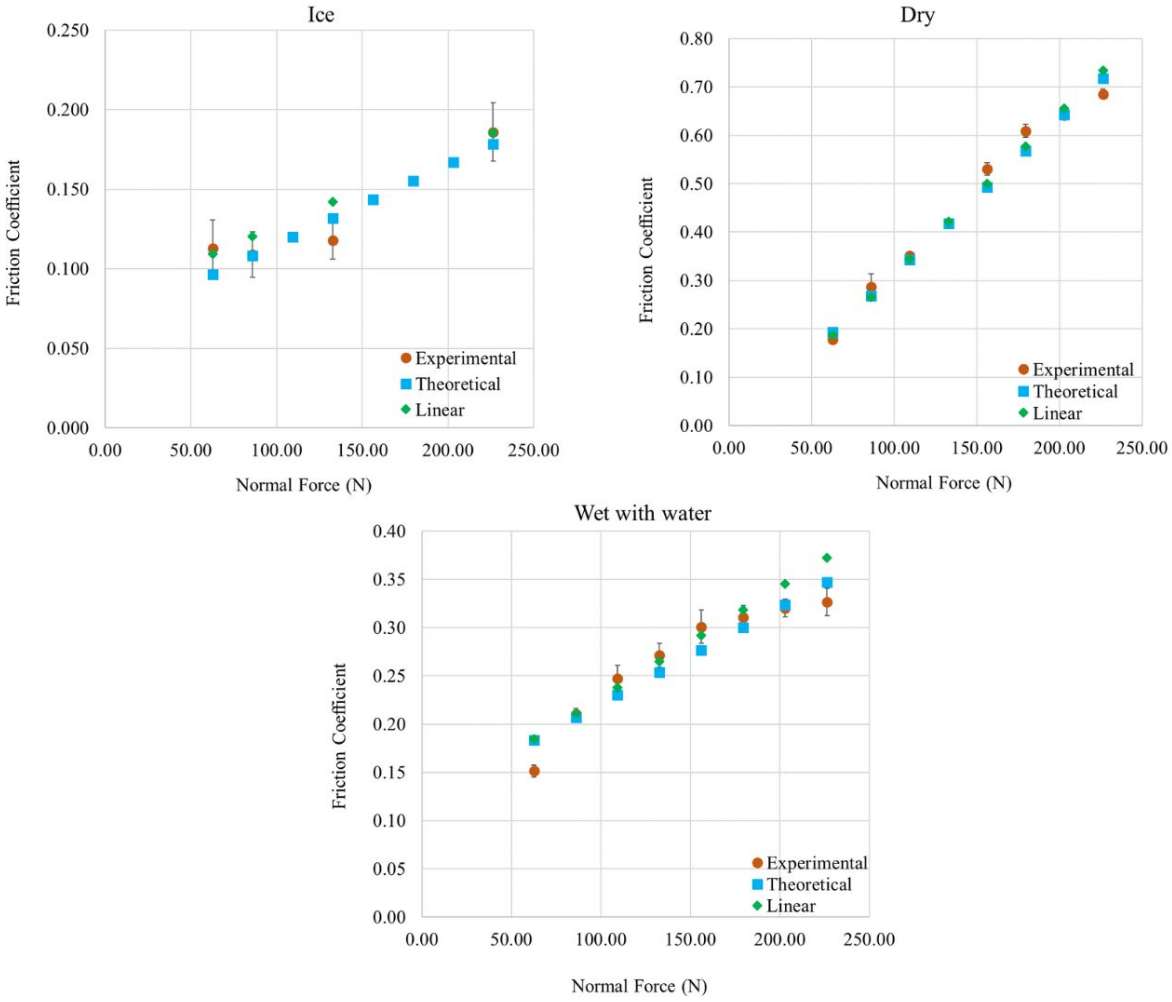

Figure 32: Results of linear and theoretical models for dry, ice, and wet concrete conditions

4.6 Conclusions

In this chapter, we successfully employed the MTA to simulate the interaction between aircraft wheels (rubber) and a runway contaminated by icing precipitation (concrete) using the methodology outlined in Chapter 3. The results validated the MTA's performance and its effectiveness in measuring friction under specific normal force and velocity condition.

The analysis confirms the device's reliability in capturing realistic wear and friction phenomena. The MTA's performance, particularly in replicating runway friction levels for ice, wet and dry conditions, aligns well with established benchmarks.

For the remaining winter conditions (removed snow, and snow), the analysis moved toward the friction behaviour under snow contaminated surfaces. Concepts such as compaction, density and moisture content were considered to evaluate the low friction coefficient values that were obtained during MTA normal force testing. Another important aspect was the residual snow that may create a lubricating layer that reduce the direct contact between the rubber and the concrete surface, and thus, lowering friction. Additionally, the high variability in texture and roughness of the concrete samples complicate friction assessment introducing another layer of complexity.

Additionally, the tested RDP in both anti-icing and de-icing modes exhibited the expected behaviors over time. PG Hybrid demonstrated the best anti-icing performance, maintaining stable friction levels throughout the test, aligning with results from similar research studies. KFO results under removed snow conditions followed the expected behavior described in comparable studies. The tests confirmed their ability to maintain surface friction on icy runways, delaying and melting ice and snow formations. While some deviations in friction values were observed, possibly due to the testing setup, the MTA effectively evaluated RDP performance under simulated winter conditions.

Our analysis of the experimental data further supports the validation of the MTA. Specifically, based on the development of the theoretical model, which applies Bowden's theory to describe the area of plastic or elastic flow by scaling the relationship between load and indentation geometry, our results align with the theory, yielding an exponent of 0.74. This demonstrates that the rubber surface is aging over time due to contact with the concrete surface, reflecting a non-purely elastic or plastic behaviour.

For ice and wet conditions, the theoretical model performed better than the linear model, with error percentages of 7.8% and 6.8%, respectively. Under wet conditions, the friction coefficient fluctuates more, and both models exhibit slightly higher average errors, suggesting that water introduces additional variability. In dry conditions, both models perform best, with the lowest average error (4.5%). The largest discrepancies between experimental and predicted friction coefficients occur under icy conditions,

particularly at lower normal forces. However, in general the experimental and predicted values align more closely at higher normal forces. Overall, the results confirm the predictive capabilities of both models.

Chapter 5: Conclusions and Recommendations

5.1 Conclusions of this dissertation

Braking performance is critical for ensuring aircraft control and safety during ground operations, particularly under winter conditions, where runway excursions pose significant safety risks. Contaminants at the runway-tire interface act as lubricants, affecting control, direction, and stopping distance. This study addresses the need for improved friction measurement methodologies to enhance runway safety during winter operations.

To fill this gap, we adapted the MTA device for friction measurement under controlled laboratory conditions, simulating aircraft ground operations during winter. The study began with a literature review to understand friction phenomena and existing methodologies. We then modified the MTA device, previously used for ice adhesion measurements, to suit runway friction assessments. Testing strategies, materials, and conditions, including the cold room, rubber attachments, concrete specimens, and de-icing products, were described in detail to ensure reproducibility and transparency.

The results confirmed the MTA's ability to simulate real-world conditions, with friction measurements aligning with CRFI values for dry, wet, and icy surfaces. Low standard deviations across tests ($\leqslant 0.01$) demonstrated the device's precision. The tested RDP fluid effectively delayed ice formation, as expected. The mathematical model further validated the MTA, showing alignment with theoretical values, such as a yield stress ratio of 0.4 at the sliding interface. This result, alongside Bowden's theory on contact areas, confirmed that the MTA reliably replicates runway conditions during aircraft operations.

The MTA offers a precise and straightforward alternative to existing methodologies, such as the British Pendulum Test. Its key advantages include compatibility with various contaminants, adaptability to different surfaces, cost-effectiveness, and ease of use. By meeting GRF standards and improving laboratory testing

capabilities, the MTA has the potential to influence runway condition assessment practices and enhance safety during winter operations at airports.

5.2 Recommendations

- Future research should consider the impact of different types of icing precipitation, as they may significantly influence friction and ice formation dynamics.
- Further investigation is also required to analyze the impact of solid RDPs' performance.
- Future research should incorporate more realistic materials, such as rougher concrete or polished surfaces, to evaluate surface dependency. Additionally, using a wheel tire instead of a rubber piece could provide more representative results.
- For the snow and compacted snow conditions, it is recommended to ensure snow compaction, moisture content and density during test, controlling temperature to avoid melting and refreezing effects that can create variability.
- Regarding the rubber attachment, further research is needed to evaluate how the exposure to winter contaminants affects the rubber piece material properties.
- Compare the results with additional friction studies or field data to validate the theoretical and linear models.
- Theoretical model enhancement by a deep analysis of the yield strength ratio to account for material variability.

References

1. IATA, *International Air Transport Association: Annual Safety Report*. 2022, IATA.

2. RASG-PA, *Regional Aviation Safety Group – Pan America: Annual Safety Report*, in *High Risk Categories*. 2023, International Civil Aviation Organization: https://www.icao.int/RASGPA/Pages/Library.aspx. p. 42.

3. IATA, *International Air Transport Association: 2024 Annual Safety Report*. 2025: https://www.iata.org/en/pressroom/2025-releases/2025-02-26-01/.

4. FSF, *Flight Safety Foundation: Global Safety Report Highlights Runway Safety, Turbulence Risks*, in *Corporate Jet Accident Categories*. 2023, FSF Communications Staff: https://flightsafety.org/fsf-global-safety-report-highlights-runway-safety-turbulence-risks/. p. 11.

5. EASA, *European Union Aviation Safety Agency: Annual Safety Review*. 2022, EASA: https://www.easa.europa.eu/en/newsroom-and-events/news/easa-annual-safety-review-2022-published. p. 174.

6. Tuncal, A., U. Suat, and E. Dursun, *A milestone to enhance runway safety: the new global reporting format.* Revista de Investigaciones Universidad del Quindío, 2021. **33**(1): p. 168-178.

7. Midtfjord, A. and A.B. Huseby. *Estimating runway friction using flight data*. in *Proceedings of E-Proceedings of the 30th European Safety and Reliability Conference and 15th Probabilistic Safety Assessment and Management Conference (ESREL2020 PSAM15), Research Publishing Services, Venice, Italy*. 2020.

8. Brassard, J.-D., et al., *Assessment of Runway Surface Conditions by British Pendulum Testing under the Global Reporting Format Winter Conditions.* Applied Sciences, 2022: p. 14.

9. Gandhewar, P. and H.G. Sonkusare, *Runway excursion: a problem.* IOSR J. Mech. Civ. Eng, 2014. **11**: p. 75-78.

10. Wallman, C.-G. and H. Åström, *Friction measurement methods and the correlation between road friction and traffic safety: A literature review.* Swedish National Road and Transport Research Institute, 2001. **VTI meddelande 911A**: p. 47.

11. Rasol, M., et al., *Progress and monitoring opportunities of skid resistance in road transport: A critical review and road sensors.* Remote Sensing, 2021: p. 26.

12. Kogbara, R.B., et al., *A state-of-the-art review of parameters influencing measurement and modeling of skid resistance of asphalt pavements.* Construction and Building Materials, 2016. **114**: p. 602-617.

13. Brassard, J.-D., M.M. Tremblay, and G. Momen. *Assessing the Impact of Common Winter Contaminations on Runway Surface Condition*. in *Int. Workshop on Atmospheric Icing of Structures*. 2022. Montreal, Canada: Mcgill.

14. HP, J., *Lubrication (Tribology)-A report on the present position and industry's needs. Department of Education and Science,* . Department of Education and Science. 1996.

15. Paturi, U.M.R., S.T. Palakurthy, and N. Reddy, *The role of machine learning in tribology: a systematic review.* Archives of Computational Methods in Engineering, 2023. **30**(2): p. 1345-1397.

16. Ramachandran, R., et al., *Anti-icing superhydrophobic surfaces: Controlling entropic molecular interactions to design novel icephobic concrete.* Entropy, 2016: p. 26.

17. Gohar, R. and H. Rahnejat, *Fundamentals of tribology*. 2018: World Scientific.

18. Yin, N., et al., *Tribo-informatics approaches in tribology research: A review.* Friction, 2023. **11**(1): p. 1-22.

19. Straffelini, G., *Friction and wear*. Springer Tracts in Mechanical Engineering. Springer, Cham. 2015.

20. Meng, Y., et al., *A review of recent advances in tribology.* Friction, 2020. **8**: p. 221-300.

21. Biancardo, S.A., et al., *A broad-based decision-making procedure for runway friction decay analysis in maintenance operations.* Sustainability, 2020. **12**(9): p. 21.

22. Perova, E., et al., *Methods for determining the friction coefficient of the road surface.* Mokslas–Lietuvos ateitis/Science–Future of Lithuania, 2019. **11**: p. 1-6.

23. Rado, Z. and M. Kane, *An initial attempt to develop an empirical relation between texture and pavement friction using the HHT approach.* Wear, 2014. **309**(1-2): p. 233-246.

24. Hall, J., et al., *Guide for pavement friction.* Final Report for NCHRP Project, 2009. **1**: p. 43.

25. Henry, J.J., *Evaluation of pavement friction characteristics: A Synthesis of Highway Practice*. Synthesis 291. Vol. 291. 2000, National Cooperative Highway Research Program: Transportation Research Board.

26. Lyon, C. and B. Persaud. *Safety effects of a targeted skid resistance improvement program*. in *Texture, Friction Management, and Ride Quality, Proceedings of the 87th Annual Meeting of Transportation Research Board (TRB), National Research Council, Washington DC, CD-ROM*. 2008.

27. Bray, J. *Skid accident reduction program (SKARP): Targeted crash reductions*. in *Institute of Transportation Engineers (ITE) 2003 Technical Conference and ExhibitInstitute of Transportation Engineers (ITE)*. 2003.

28. James C. Wambold, et al., *International PIARC Experiment to Compare and Harmonize Texture and Skid Resistance Measurements*. 2003, PIARC Technical Committee on Surface Characteristics C.1: World Road Association.

29. Dotan, A., et al., *The relationship between water wetting and ice adhesion.* Journal of Adhesion Science and Technology, 2009. **23**(15): p. 1907-1915.

30. Pratt, M.P. and J.A. Bonneson, *Assessing curve severity and design consistency using energy-and friction-based measures.* Transportation Research Record, 2008. **2075**(1): p. 8-15.

31. Elkhazindar, A., M. Hafez, and K. Ksaibati, *Incorporating pavement friction management into pavement asset management systems: State department of transportation experience.* CivilEng, 2022. **3**(2): p. 541-561.

32. Choubane, B., C.R. Holzschuher, and S. Gokhale, *Precision of locked-wheel testers for measurement of roadway surface friction characteristics.* Transportation Research Record, 2004. **1869**(1): p. 145-151.

33. Kumar, A., et al., *A state-of-the-art review of measurement and modelling of skid resistance: The perspective of developing nation.* Case Studies in Construction Materials, 2023: p. e02126.

34. Ward, A.B. and C.A. Rutland, *Development of Smartphone Accelerometer-Based Airfield Friction Assessment Tools.* Transportation Research Record, 2018. **2672**(23): p. 95-105.

35. Kummer, H.W. and W.E. Meyer. *Tentative skid-resistance requirements for main rural highways*. in *NCHRP Report*. 1967. United States, Pennsylvania

36. Antal, C., F. Popa, and M. Mos. *Annual Session of Scientific Papers "IMT ORADEA 2019"*. in *IOP Conference Series: Materials Science and Engineering*. 2019. Oradea, Felix SPA, Romania: IOP Conference Series: Materials Science and Engineering.

37. Kane, M. and V. Edmondson, *Skid resistance: understanding the role of road texture scales using a signal decomposition technique and a friction model.* International Journal of Pavement Engineering, 2022. **23**(2): p. 499-513.

38. Kane, M., et al., *Report on different parameters influencing skid resistance, rolling resistance and noise emissions.* TYROSAFE Deliverable D, 2009. **10**: p. 95.

39. Pasindu, H., T. Fwa, and G. Ong. *Analysis of skid resistance variation on a runway during an aircraft landing operation*. in *Seventh international conference on maintenance and rehabilitation of pavements and technological control, Auckland*. 2012.

40. Riahi, E., et al., *On-Board Evaluation of Pavement Wetness from Water Spray.* Engineering Proceedings, 2023. **36**(1): p. 5.

41. Nataadmadja, A.D., et al., *Correlating laboratory test methodologies to measure skid resistance of pavement surfaces.* Transportation Research Record, 2015. **2506**(1): p. 107-115.

42. Oliver, J.W., *Factors affecting the correlation of skid-testing machines and a proposed correlation framework.* Road & Transport Research: A Journal of Australian and New Zealand Research and Practice, 2009. **18**(2): p. 39-48.

43. Wilson, D.J., *An analysis of the seasonal and short-term variation of road pavement skid resistance*, in ***Department of Civil and Environmental Engineering***. 2006, ResearchSpace@ Auckland: University of Auckland. p. 17.

44. Kumar, B. and D. Wilson. *Prediction of pavement surface skid resistance and the effect of smaller chip size*. in *IPENZ Transportation Group Conference, Christchurch*. 2010.

45. ISO, *International Organization for Standardization: 12473-1: Characterization of Pavement Texture by Use of Surface Profiles*. 1997, ISO 13473-1:2019. p. 43.

46. Congresses, P.I.A.o.R. *Report of the committee on surface characteristics*. in *XVIII World Road Congress*. 1987. World Road Association Paris.

47. Faghihnejad, A. and H. Zeng, *Fundamentals of surface adhesion, friction, and lubrication*. Polymer Adhesion, Friction, and Lubrication. 2013. 1-57.

48. Li, H., et al., *Dynamic variation and deterioration mechanism of the friction coefficient between tire and pavement under the icy and snowy circumstances.* International Journal of Pavement Engineering, 2022: p. 1-13.

49. Bleszynski, M. and E. Clark, *Current Ice Adhesion Testing Methods and the Need for a Standard: A Concise Review.* Standards, 2021. **1**(2): p. 117-133.

50. Wang, D., et al., *Influence of the gritting material applied during the winter services on the asphalt surface performance.* Cold Regions Science and Technology, 2015. **112**: p. 39-44.

51. U.S. Department of Transportation Federal Aviation Administration, F.A., *Airport Field Condition Assessments and Winter Operations Safety*, in *150/5200-30D*. 2020.

52. Bylica, A. and A. Pashkevich, *Introduction of Global Reporting Format: Summary of the First Winter Season in Poland.* Sustainability, 2022: p. 15.

53. Klein-Paste, A., *Airplane braking friction on dry snow, wet snow or slush contaminated runways.* Cold regions science and technology, 2018. **150**: p. 70-74.

54. Rosta, S. and L. Gáspár, *Skid Resistance of Asphalt Pavements.* Eng, 2023. **4**(2): p. 1597-1615.

55. Chu, L., et al., *Directional skid resistance characteristics of road pavement: implications for friction measurements by British pendulum tester and dynamic friction tester.* Transportation research record, 2019. **2673**(10): p. 793-803.

56. Chu, L., W. Guo, and T. Fwa, *Theoretical and practical engineering significance of British pendulum test.* International Journal of Pavement Engineering, 2022. **23**(1): p. 1-8.

57. ASTM, *E303 Standard Test Method for Measuring Surface Frictional Properties Using the British Pendulum Tester*. 1993. p. 7.

58. Yu, M., et al., *Measurement and modeling of skid resistance of asphalt pavement: A review.* Construction and building materials, 2020. **260**: p. 119878.

59. Kane, M. and V. Cerezo, *A contribution to tire/road friction modeling: From a simplified dynamic frictional contact model to a "Dynamic Friction Tester" model.* Wear, 2015. **342**: p. 163-171.

60. Ueckermann, A., et al., *Calculation of skid resistance from texture measurements.* Journal of traffic and transportation engineering (English edition), 2015. **2**(1): p. 3-16.

61. Tan, T., et al., *Safety aspects on icy asphalt pavement in cold region through field investigations.* Cold regions science and technology, 2019. **161**: p. 21-31.

62. Do, M.-T., et al., *Pavement polishing—Development of a dedicated laboratory test and its correlation with road results.* Wear, 2007. **263**(1-6): p. 36-42.

63. Hofko, B., et al. *Correlating field and lab measurements of skid resistance by skiddometer and Wehner/Schulze device*. in *Proceedings of the Annual Meeting of Transportation Research Board, Washington, DC, USA*. 2017.

64. Rekilä, K., *Bicycle braking friction measurements on winter roads*, in *Civil and Environmental Engineering*. 2015, Aalto University. p. 81.

65. Marvin, J. and J. Drake, *Evaluation of Methods Used for Measuring the Slip and Skid Resistance of Permeable Interlocking Concrete Pavement under Winter Conditions.* 2th International Conference on Concrete Block Pavement Seoul, Korea, 2018.

66. Drake, J., J. Marvin, and J. Scott, *De-icing Operations for Permeable Interlocking Concrete Pavements.* In Transportation Association of Canada 2021 Conference and Exhibition-Recovery and Resilience: Transportation after COVID-19., 2021.

67. ASTM, *American Society for Testing and Materials: E670-09*, in *Standard Test Method for Testing Side Force Friction on Paved Surfaces Using the Mu-Meter*. 2020, ASTM. p. 12.

68. ASTM, *E2340/E2340M-11: Standard Test Method for Measuring the Skid Resistance of Pavements and Other Trafficked Surfaces Using a Continuous Reading, Fixed-Slip Technique.* , in *ASTM*. 2023. p. 6.

69. ASTM, *E3304-22 Standard Test Method for Measuring the Skid Resistance of Pavements and Other Trafficked Surfaces Using a Walking Speed Continuous Friction-Measuring Equipment (CFME) Fixed-Slip Technique*. 2022. p. 5.

70. Al-Qadi, I.L., et al., *Feasibility of using friction indicators to improve winter maintenance operations and mobility*. 2002, NCHRP Web Document 53 (Project 6-14): Contractor's Final Report: Transportation Research Board, National Research Council Washington, DC, USA. 151.

71. Gerthoffert, J., et al., *A Brush-based approach for modelling runway friction assessment device.* International Journal of Pavement Engineering, 2020. **21**(13): p. 1694-1702.

72. Andriejauskas, T., V. Vorobjovas, and V. Mielonas, *Evaluation of skid resistance characteristics and measurement methods.* The 9th International Conference "Environmental Engineering 2014", 2014. **9**: p. 1.

73. Shafii, M.A., *Skid resistance and the effect of temperature*, in *Civil Engineering*. 2009, Universiti Teknologi Malaysia.

74. Transports, M.C.d. *Instrument de Mesure Automatique de la Glissance (IMAG) ASTM E2100-04*. FR5I2455.CR2 2024; Skid resistance friction trailer]. Available from: https://phototheque.aviation-civile.gouv.fr/Main.htm.

75. Kleine-Beek, W., *Runway Friction Characteristics Measurement and Aircraft Braking (RuFAB)*, in *EASA.2008.C46*. 2010, BMT Fleet Technology Limited: Kanata, ON.

76. Yan, Y., et al., *Spectral techniques applied to evaluate pavement friction and surface texture.* Coatings, 2020: p. 13.

77. Jepriando, T., D. Priambodo, and M.K. Harso, *ANALYSIS OF SKID-RESISTANT RUNWAY PAVEMENT SURFACE ON YOGYAKARTA INTERNATIONAL AIRPORT WITH MU-METER TEST METHOD.* Advances in Transportation and Logistics Research, 2022. **5**: p. 1048-1059.

78. Iwanowski, P., K. Blacha, and M. Wesołowski. *Review of modern methods for continuous friction measurement on airfield pavements*. in *IOP Conference Series: Materials Science and Engineering*. 2018. IOP Publishing.

79. Kallio, M. *Moventor Skiddometer BV-11*. 2022; Available from: https://moventor.com/skiddometer-bv11-2/.

80. Administration, F.A., *Measurement, construction and maintenance of skid resistant airport pavement surfaces*, in *Federal Aviation Administration Advisory Circular No. 150/5200-30D*. 2020.

81. Ltd, T.S. *Mk 3 Electronic Decelerometer*. 2023 [cited 2024; Available from: https://www.tesinstruments.com/.

82. Canada, T. *Transport Canada: Advisory Circular (AC) No. 302-026*. 2017.

83. Canada, T., *Advisory Circular (AC) No. 300-019. Global Reporting Format (GRF) for Runway Surface Conditions*. 2021, Transport Canada: https://tc.canada.ca/en/aviation/reference-centre/advisory-circulars/advisory-circular-ac-no-300-019.

84. *An Evaluation of Winter Operational Runway Friction Measurement Equipment, Procedures, and Research*. 1995, Winter Runway Friction Measurement and Reporting Working Group. p. 80.

85. ICAO, *International Civil Aviation Organization: Airport Services Manual - Part II - Pavement Surface Conditions (Doc 9137P2)*. 2002: ICAO store.

86. McCall, B.M. and D. Kroeger, *Highway Maintenance Concept Vehicle Final Report: Phase Three*, in *Center for Transportation Research and Education Iowa State University*. 2001, Iowa State University. p. 170.

87. *Transportation Safety Board of Canada: Aviation Investigation Report A10A0032*. 2010.

88. Sabey, B.E. and G. Lupton, *Friction on wet surfaces of tire-tread-type vulcanizates.* Rubber Chemistry and Technology, 1964. **37**(4): p. 878-893.

89. Yun, D., L. Hu, and C. Tang, *Tire–Road Contact Area on asphalt concrete pavement and its relationship with the skid resistance.* Materials, 2020. **13**(3): p. 615.

90. Xu, X., et al., *Long-term skid resistance evaluation of GAC-16 based on accelerated pavement testing.* Advances in Materials Science and Engineering, 2020(1): p. 9.

91. Omar, L.G. *Investigating the influence of distress on long-term performance of pavement friction of rural roads in Onratio Canada*. in *TRB 2019 Annual Meeting, Washington DC*. 2019.

92. Hofko, B., et al., *A laboratory procedure for predicting skid and polishing resistance of road surfaces.* International Journal of Pavement Engineering, 2019. **20**(4): p. 439-447.

93. Wang, H., I.L. Al-Qadi, and I. Stanciulescu, *Effect of surface friction on tire–pavement contact stresses during vehicle maneuvering.* Journal of Engineering Mechanics, 2014. **140**(4): p. 04014001.

94. Niu, Y., et al., *Techniques and methods for runway friction measurement: A review of state of the art.* IEEE Transactions on Instrumentation and Measurement, 2021. **70**: p. 1-17.

95. Liu, Y., R. Wang, and T. Wan, *A method determining critical operating parameters for landing aircraft based on runway pavement skid resistance.* International Journal of Pavement Engineering, 2024. **25**(1): p. 2346286.

96. Brassard, J.-D., et al., *New insights into icephobic material assessment: Introducing the human motion–inspired automated apparatus (HMA).* Cold Regions Science and Technology, 2025. **229**: p. 104351.

97. ASTM, *Slip Resistance Test Safety Criteria ASTM E303*.

98. Transport Canada: Ottawa, O., Canada, *Guidelines for Aircraft Ground- Icing Operations- TP 14052*.

99. De, S.K. and J.R. White, *Rubber technologist's handbook*. Vol. 1. 2001: iSmithers Rapra Publishing.

100. Sethuraj, M.R. and N.T. Mathew, *Natural rubber: biology, cultivation and technology*. 2012: Elsevier.

101. Ido, T., et al., *Sliding friction characteristics of styrene butadiene rubbers with varied surface roughness under water lubrication.* Tribology International, 2019. **133**: p. 230-235.

102. Santos, P.M.D. and E.N.B.S. Júlio, *Comparison of Methods for Texture Assessment of Concrete Surfaces.* ACI Materials Journal, 2010. **107**(5).

103. Sarker, M., D. Dias-da-Costa, and S.A. Hadigheh, *Multi-scale 3D roughness quantification of concrete interfaces and pavement surfaces with a single-camera set-up.* Construction and Building Materials, 2019. **222**: p. 511-521.

104. *ISO 4287: 1997, International Organization for Standardization 4287: Geometrical Product Specifications (GPS) , Surface texture: Profiling method – Terms, definitions and surface texture parameters.*

105. Cntech. *Profilm3 Optical Profiler*. 2009; Available from: https://www.cntech.co.uk/p/profilm3d-optical-profiler.

106. Li, H., et al., *Dynamic variation and deterioration mechanism of the friction coefficient between tire and pavement under the icy and snowy circumstances.* International Journal of Pavement Engineering, 2023. **24**(2): p. 2148160.

107. Klein-Paste, A., *Runway Operability under Cold Weather Conditions. Tire-pavement friction creation by sand particles on iced pavements, and non-contacting detection of sand particles on pavements.* 2007.

108. Baimukhametov, G. and G. White, *Review and Improvement of Runway Friction and Aircraft Skid Resistance Regulation, Assessment and Management.* Applied Sciences, 2025. **15**(2): p. 548.

109. Keropyan, A. and A.Y. Albagachiev, *Study of the Main Factors Affecting the Increase in the Friction Coefficient of Interacting Surfaces of Rail Vehicles.* Journal of Machinery Manufacture and Reliability, 2024. **53**(3): p. 208-211.

110. Sun, B., *Unveiling the True Nature of Sliding Friction through Thermodynamic Principles.* 2024.

111. Dowson, D., *History of Tribology, London, NY.* Addison-Wesley Longman Limited, 1979.

112. Bowden, F.P. and D. Tabor, *The friction and lubrication of solids*. Vol. 1. 2001: Oxford university press.

113. *MATERIAL PROPERTIES OF CONCRETE*, https://www.in.gov/dot/div/contracts/standards/dm-Archived/09Metric/Part6/Ch62/figures/Fig62-1A.pdf, Editor.:

https://www.in.gov/dot/div/contracts/standards/dm-Archived/09Metric/Part6/Ch62/figures/Fig62-1A.pdf.

114. Mehdi, A.H., et al., *STUDYING THE MECHANICAL PROPERTIES OF TIRE RUBBER BEFORE AND AFTER CONSUMPTION.* 2024.